



Oxygen isotope ratios of FeO-poor chondrules in CR3 chondrites: Influence of dust enrichment and H₂O during chondrule formation

Travis J. Tenner^{a,*}, Daisuke Nakashima^{a,1}, Takayuki Ushikubo^{a,2},
Noriko T. Kita^a, Michael K. Weisberg^{b,c}

^a *WiscSIMS, Department of Geoscience, University of Wisconsin-Madison, Madison, WI 53706, USA*

^b *Kingsborough Community College and Graduate Center, The City University of New York, 2001 Oriental Boulevard, Brooklyn, NY 11235-2398, USA*

^c *American Museum of Natural History, Central Park West at 79th Street, New York, NY 10024-5192, USA*

Received 14 February 2014; accepted in revised form 12 September 2014; available online 15 October 2014

Abstract

We present detailed electron microprobe analyses and oxygen three-isotope measurements by high precision secondary ion mass spectrometry on 45 type I (FeO-poor) chondrules/fragments and 3 type II (FeO-rich) chondrule fragments from Meteorite Hills 00426 and Queen Alexandra Range 99177, two of the most primitive CR3 chondrites. Type I chondrules/fragments have Mg#’s (defined as the Mg# of constituent olivine and/or low-Ca pyroxene) ranging from 94.2 to 99.2; type II chondrule fragments have Mg#’s of 53–63. Oxygen three-isotope measurements plot on the slope ~1 primitive chondrule mineral (PCM) line. Within chondrules, $\Delta^{17}\text{O}$ ($=\delta^{17}\text{O}-0.52 \times \delta^{18}\text{O}$) values of coexisting olivine, pyroxene, and plagioclase are homogeneous, with propagated uncertainties of 0.3‰. This indicates each phase crystallized from the final chondrule melt, and that efficient oxygen isotope exchange occurred between ambient gas and chondrule melt. Among type I chondrules there is a well-defined increase in $\Delta^{17}\text{O}$, from -5.9‰ to $\sim -1\text{‰}$, as Mg#’s decrease from 99.2 to ~ 96 ; type II chondrule fragments are comparatively ¹⁶O-poor ($\Delta^{17}\text{O}$: $\sim 0.2\text{--}0.6\text{‰}$). The relationship between Mg# and $\Delta^{17}\text{O}$ among type I chondrules confirms that addition of a ¹⁶O-poor oxidizing agent to the highest Mg# chondrule precursors resulted in forming lower Mg# CR chondrules. Using aspects of existing equilibrium condensation models and a mass balance we estimate that type I CR chondrules formed at dust enrichments of 100–200 \times , from dusts with 0–0.8 times the atomic abundance of ice, relative to CI dust. The type II chondrule fragments are predicted to have formed at CI dust enrichments near 2500 \times .

© 2014 Elsevier Ltd. All rights reserved.

1. INTRODUCTION

Chondrules are ubiquitous (20–80 volume percent) in primitive chondrites (Scott et al., 1996). Their igneous textures and spherulitic morphologies indicate rapid heating and crystallization of pre-existing solids (Tsuchiyama et al., 1980; Hewins and Radomsky, 1990; Jones et al., 2000, 2005) within the inner regions of the protoplanetary disk (Cassen, 2001; Desch and Connolly, 2002). Chondrules from the least metamorphosed chondrites display a wide

* Corresponding author. Tel.: +1 608 262 8960; fax: +1 608 262 0693.

E-mail address: tenner@wisc.edu (T.J. Tenner).

¹ Present address: Department of Earth and Planetary Material Sciences, Faculty of Science, Tohoku University, Aoba, Sendai, Miyagi 980-8578, Japan.

² Present address: Kochi Institute for Core Sample Research, Japan Agency for Marine-Earth Science and Technology (JAMSTEC), 200 Monobe Otsu, Nankoku City, Kochi 783-8502, Japan.

range of FeO contents in their constituent olivines and pyroxenes. Mg#’s (mol.% MgO/[MgO + FeO]) of chondrule olivines and pyroxenes range from 40 to 100 (McSween, 1977; Jones and Scott, 1989; Scott and Jones, 1990; Jones, 1990, 1994, 1996; Kallemeyn et al., 1994; Kurahashi et al., 2008; Connolly and Huss, 2010; Kita et al., 2010; Libourel and Chaussidon, 2011; Ushikubo et al., 2012; Schrader et al., 2013; Tenner et al., 2013). This indicates the redox state of the chondrule-forming environment varied significantly, based on metal–silicate phase equilibria (Kring, 1988; Zanda et al., 1994). In particular, type I chondrules, defined as those with olivine or low-Ca pyroxene Mg#’s between 90 and 100 (Jones et al., 2005) formed at more reducing conditions ($\log f_{\text{O}_2}$: IW -6 to IW -2) than type II (mafic mineral Mg# < 90) chondrules ($\log f_{\text{O}_2}$: IW -2 to IW; IW = iron-wüstite buffer). As a whole, chondrules formed at more oxidizing conditions than Ca, Al-rich inclusions, or CAIs ($\log f_{\text{O}_2} < \text{IW} -6$; Grossman et al., 2008), suggesting their environments were most likely enhanced in oxygen-rich dust (Wood, 1967). Imposed oxygen fugacities were probably controlled by the degree of dust enrichment, relative to the Solar gas, and by the amount of H₂O and carbon in solid precursors (Connolly et al., 1994; Ebel and Grossman, 2000; Fedkin and Grossman, 2006; Grossman et al., 2012; Fedkin et al., 2012). The Mg# of a chondrule reflects these parameters.

In primitive chondrites oxygen isotope ratios of chondrules are linked to the values of their precursors, and conceivably document exchange between ambient gas and chondrule melt. Specifically, homogeneous oxygen isotope ratios among silicate phases from individual chondrules infer the value of the final chondrule melt, and suggest oxygen isotope ratios did not change during and after crystallization (e.g. Ushikubo et al., 2012). Chondrules from primitive carbonaceous chondrites plot on a slope ~ 1 line when comparing $\delta^{18}\text{O}$ and $\delta^{17}\text{O}$ (where $\delta^{17,18}\text{O}$ (‰) = $[(R_{\text{sample}}/R_{\text{VSMOW}}) - 1] \times 1000$; $R = ^{17,18}\text{O}/^{16}\text{O}$; VSMOW = Vienna Standard Mean Ocean Water; Baertschi, 1976) and show an appreciable range ($\delta^{17,18}\text{O}$: ~ -20 ‰ to $+5$ ‰; Clayton, 1993; Jones et al., 2000, 2004; Kunihiro et al., 2004, 2005; Krot et al., 2006a, 2010; Connolly and Huss, 2010; Libourel and Chaussidon, 2011; Rudraswami et al., 2011; Ushikubo et al., 2012; Schrader et al., 2013; Tenner et al., 2013) (Fig. 1), which is distinct from the relatively small variability in oxygen isotope ratios of chondrules from ordinary and E3 chondrites (Clayton et al., 1991; Kita et al., 2010; Weisberg et al., 2011). Ushikubo et al. (2012) defined the primitive chondrule mineral (PCM) line as having a $\delta^{18}\text{O}$ versus $\delta^{17}\text{O}$ slope of 0.987 ± 0.013 , based on high precision secondary ion mass spectrometry (SIMS) measurements of chondrules from Acfer 094, one of the least metamorphosed carbonaceous chondrites (Grossman and Brearley, 2005). This slope is unique when compared to oxygen isotope ratios in terrestrial materials, and likely originated through mass-independent fractionation processes early in the Solar System (Thiemens and Heidenreich, 1983; Yurimoto and Kuramoto, 2004; Lyons and Young, 2005; Young et al., 2008; Lyons et al., 2009; Chakraborty et al., 2013). Such

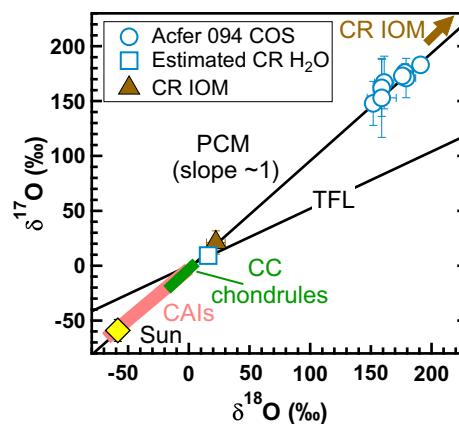


Fig. 1. Illustrative oxygen three-isotope diagram of chondritic materials. The slope ~ 1 primitive chondrule minerals (PCM) line from Ushikubo et al. (2012) is shown for reference. Also shown is the terrestrial fractionation line (TFL). The shaded region for CAIs represents data from Clayton (1993) and Gounelle et al. (2009), and extends near the TF line. The shaded region for carbonaceous chondrite (CC) chondrules represents data from Jones et al. (2000, 2004), Kunihiro et al. (2004, 2005), Krot et al. (2006a), Connolly and Huss (2010), Libourel and Chaussidon (2011), Rudraswami et al. (2011), Ushikubo et al. (2012), Schrader et al. (2013), and Tenner et al. (2013). The estimated O-isotope ratio for the Sun is taken from McKeegan et al. (2011). Data from Acfer 094 cosmic symplectites (COS), which are inferred to sample O-isotope ratios of H₂O, are from Sakamoto et al. (2007). The estimated O-isotope ratio of H₂O in CR chondrites is from Clayton and Mayeda (1999), based on matrix and whole-rock measurements. The CR insoluble organic material (IOM) datum is from Hashizume et al. (2011) and is the average of areas #1 and #2 in their study; some CR IOM has extreme $\delta^{17,18}\text{O}$ values, exceeding $+400$ ‰. Uncertainties are 2SD.

processes could be responsible for the large variations of oxygen isotope ratios in chondritic materials, including ^{16}O -rich CAIs and chondrules with $\delta^{17,18}\text{O}$ values down to ~ -75 ‰ (Kobayashi et al., 2003; Gounelle et al., 2009) and ^{16}O -poor cosmic symplectites (Fe, Ni metal and sulfides oxidized by H₂O; Sakamoto et al., 2007) and organic material (Hashizume et al., 2011), with positive $\delta^{17,18}\text{O}$ values up to several hundred per mil (Fig. 1). In relation to these materials, chondrules from carbonaceous chondrites are intermediate in $\delta^{17}\text{O}$ and $\delta^{18}\text{O}$ (Fig. 1). Thus, it is conceivable that chondrule values, and their range of values, were influenced by mixing of ^{16}O -rich and ^{16}O -poor precursors (e.g. Clayton et al., 1983). The presence of isotopically distinct “relict” mineral grains in chondrules, which are either ^{16}O -rich or ^{16}O -poor relative to minerals that crystallized from the final “host” chondrule melt (Kunihiro et al., 2004, 2005; Wasson et al., 2004; Connolly and Huss, 2010; Rudraswami et al., 2011; Ushikubo et al., 2012; Schrader et al., 2013; Tenner et al., 2013) supports this hypothesis.

Within many primitive carbonaceous chondrites, type I chondrules are enriched in ^{16}O when compared to type II chondrules (Jones et al., 2000, 2004; Kunihiro et al., 2004, 2005; Krot et al., 2006a, 2006b; Connolly and Huss, 2010; Nakashima et al., 2010; Rudraswami et al., 2011; Ushikubo et al., 2012; Schrader et al., 2013; Tenner et al.,

2013). This relationship led [Connolly and Huss \(2010\)](#) to hypothesize that addition of ^{16}O -poor H_2O (e.g. [Fig. 1](#)) to FeO-poor chondrule precursors, along with increases in dust enrichment, contributed to an oxidized environment that formed comparatively FeO-rich chondrules. If true, one might expect to observe a systematic relationship between Mg#s and oxygen isotope ratios of chondrules, particularly among type I chondrules, as metal–silicate phase equilibria predicts a four-order of magnitude increase in $f\text{O}_2$ as chondrule Mg#s decrease from 100 to 90. However, such a relationship is not clearly defined among current type I chondrule datasets because either (1) they lack detailed Mg#s; (2) not enough data exist within a given study; (3) the chondrules studied encompass a limited Mg# range (e.g. type I chondrules measured by [Ushikubo et al., 2012](#) and [Tenner et al., 2013](#) mainly have Mg#s > 98, while a few have Mg#s near 95); or (4) Mg# data are compromised by Fe–Mg diffusion during thermal metamorphism (e.g. Allende CV3.6 chondrules measured by [Rudraswami et al., 2011](#)). As a result, we have chosen to investigate Mg# and O-isotope systematics from a large suite of type I chondrules in pristine, CR3.0 chondrites by scanning electron microscopy (SEM), electron microprobe analysis (EMP), and SIMS. CR3.0 chondrites are ideal for this undertaking because they lack evidence of thermal metamorphism and aqueous alteration ([Abreu and Brearley, 2010](#)), and because CR chondrites are dominated by type I chondrules with a more complete range of Mg#s ([Weisberg et al., 1993](#)). By determining the relationship between Mg#s and oxygen isotope ratios of type I CR chondrules, our goal is to more clearly understand the environment from which they formed.

2. SAMPLE SELECTION AND ANALYTICAL TECHNIQUES

Meteorite Hills (MET) 00426 and Queen Alexandra Range (QUE) 99177 CR chondrites were chosen for investigation. Their mineralogic and petrologic characteristics (i.e. ubiquitous amorphous material and nanosulfides in matrices and fine-grained rims, preserved unaltered chondrule glass, and very low abundances of phyllosilicates and calcite in matrices) indicate they escaped significant thermal metamorphism and aqueous alteration, leading to their classification as rare, petrologic type 3.00 chondrites ([Abreu and Brearley, 2010](#)). CR chondrites also have abundant type I chondrules with olivine compositions ranging from $\text{Fo}_{90-99.5}$ ([Weisberg et al., 1993](#)). Thin sections MET 00426,46 and QUE 99177,49 were obtained for characterization.

2.1. Scanning electron microscopy

Chondrule petrography was examined with a Hitachi S-3400 N SEM equipped with an energy dispersive X-ray spectrometer (EDS). Regions from phenocrysts that were free of cracks, pits and inclusions were identified as targets for EMP and SIMS analysis. When possible, we located regions of interest from both multiple phenocrysts and multiple phases per chondrule.

2.2. Electron microprobe analysis

Major element oxide (SiO_2 , TiO_2 , Al_2O_3 , Cr_2O_3 , FeO , MnO , MgO , CaO , Na_2O , and K_2O) concentrations of crystalline phases were obtained with a Cameca SX-51 electron microprobe (EMP) using a 15 keV accelerating voltage, a 10 nA beam current, a fully focused beam, and respective peak and background counting times of 10 and 5 s. Standards consisted of olivine ($\text{Fo}_{0, 83, 89, 100}$), pyroxene (enstatite, diopside, wollastonite, augite, jadeite and omphacite), plagioclase ($\text{An}_{0, 18, 49, 67, 78, 95}$), rutile, hornblende, chromite, hematite, tephroite, and microcline. Data reduction, including a $\phi(\rho Z)$ matrix correction, was performed with Probe for Windows software. For plagioclase, Na count rates were monitored using albite-rich endmember standards, and no appreciable drop-off was observed under analytical conditions. Calculated detection limits (at 99% confidence) are 0.06, 0.05, 0.05, 0.06, 0.09, 0.08, 0.05, 0.04, 0.05, and 0.03 wt.%, respectively, for the oxides listed above. During sessions olivine, pyroxene, and plagioclase standards were periodically analyzed as unknowns to ensure that appropriate concentrations and totals of 99–101 wt.% were achieved, and that cations were within 0.01 of ideal stoichiometry. Line traverses of EMP analyses were collected at the exact locations of subsequent SIMS analyses.

2.3. Oxygen three-isotope analysis by SIMS

In-situ oxygen three-isotope measurements of olivine, pyroxene, and plagioclase in chondrules were acquired with the Cameca IMS 1280 SIMS at the University of Wisconsin-Madison. Analytical methods are similar to those described in [Kita et al. \(2010\)](#). The primary Cs^+ beam was tuned to produce a 15 μm diameter spot with a primary ion intensity of ~ 3 nA. Secondary ions of ^{16}O , ^{17}O , and ^{18}O were detected with three Faraday cups simultaneously, with rates of $\sim 2.5 \times 10^9$, $\sim 1 \times 10^6$, and $\sim 5 \times 10^6$ counts per second (cps), respectively. Mass resolving power (MRP at 10% peak height) was set to ~ 2200 for ^{16}O and ^{18}O using two detectors on the multi-collection array, and 5000 for ^{17}O using a mono-collector at a fixed position. Following each analysis $^{16}\text{O}^1\text{H}$ was monitored to determine its contribution to the ^{17}O signal (e.g. [Heck et al., 2010](#)) and was calculated to have an effect of less than 0.1‰, with a typical contribution of $\sim 0.01\%$.

External reproducibility was established and intermittently monitored by measurements of a San Carlos olivine standard ($\delta^{18}\text{O} = 5.32\%$ VSMOW; [Kita et al., 2010](#)), where 8 standard analyses, 4 before and 4 after, bracketed 10–15 analyses of unknowns ([Kita et al., 2009](#)). External reproducibility is calculated as twice the standard deviation (2SD) of San Carlos olivine bracketing measurements (n : 31 brackets), with average values of 0.3, 0.4 and 0.4‰ for $\delta^{18}\text{O}$, $\delta^{17}\text{O}$, and $\Delta^{17}\text{O}$ ($=\delta^{17}\text{O}-0.52 \times \delta^{18}\text{O}$), respectively. The external reproducibility in $\delta^{17}\text{O}$ is similar to the internal error in $\delta^{17}\text{O}$, and is consistent with the thermal background noise (400 cps per 100 s integration; 1SD) from the FC detector. However, the external reproducibility in $\delta^{18}\text{O}$ exceeds the respective internal error of a single analy-

sis (typically 0.1‰), indicating the instrumental bias varies from one spot to the next (e.g. [Kita et al., 2009](#)). As a result, we assign the bracketing 2SD to represent the uncertainty of a single analysis. For reference, internal errors among standards and unknowns were indistinguishable. As such, we did not include internal error in the spot to spot uncertainty.

Instrumental biases due to variability in olivine and pyroxene compositions were assessed by measuring Fo_{60-100} , low-Ca pyroxene (En_{85-97}), and diopside (Wo_{50}) standards with known $\delta^{18}\text{O}_{\text{VSMOW}}$ values, and by establishing calibration curves normalized relative to the bias of the San Carlos olivine bracketing standard ([Appendix EA1](#)). Endmember ranges of standards cover the compositions of nearly all unknowns measured. Differences in the bias correction as a function of endmember component for Fo_{60-100} , En_{85-100} , and Wo_{0-50} are, at a maximum, 0.5‰, 0.9‰, and 2.8‰, respectively ([Appendix EA1](#)). For plagioclase measurements a constant 2.0‰ bias correction was applied, based on an An_{95} standard. This is appropriate given that unknowns are near An_{95} in composition.

To assess the degree of homogeneity of chondrule oxygen isotope ratios, multiple SIMS analyses were collected per chondrule ($n = 3$ to 14; average: 8). This is particularly important because chondrules from carbonaceous chondrites often have olivines with heterogeneous oxygen isotope ratios ([Kunihiro et al., 2004, 2005](#); [Wasson et al., 2004](#); [Connolly and Huss, 2010](#); [Rudraswami et al., 2011](#); [Ushikubo et al., 2012](#); [Schrader et al., 2013](#); [Tenner et al., 2013](#)), indicating they did not crystallize from the final chondrule melt. Such olivines likely attained their oxygen isotope signatures from a previous generation of melting and crystallization of solid precursors; grains then remained partially or fully intact during the final chondrule-forming event. Their oxygen isotope signatures were preserved because of low oxygen diffusion rates in olivine at chondrule-forming conditions (e.g. [Chakraborty, 2010](#)). Such olivines are commonly defined as “relicts”; their data are excluded when determining the “host” oxygen isotope ratio of a chondrule, defined as that representing the bulk value of the final chondrule melt. Similar to [Ushikubo et al. \(2012\)](#) and [Tenner et al. \(2013\)](#), we define relict olivines as those with $\Delta^{17}\text{O}$ values exceeding the 3SD external reproducibility (in this study, 0.6‰) when compared to the averaged “host” $\Delta^{17}\text{O}$ value of a chondrule.

Uncertainties of averaged $\delta^{18}\text{O}$ and $\delta^{17}\text{O}$ per chondrule are taken as the propagation of (1) the 2 standard error (2SE) of chondrule analyses ($=2\text{SD}/\sqrt{\text{number of analyses}}$); (2) the 2SE of associated San Carlos olivine bracketing analyses, which accounts for uncertainty in the matrix correction (e.g. [Appendix EA1](#)); and (3) the uncertainty due to sample topography and/or sample positioning on the SIMS stage, estimated to be 0.3‰ for $\delta^{18}\text{O}$ and 0.15‰ for $\delta^{17}\text{O}$ ([Kita et al., 2009](#)). The propagated uncertainty in $\Delta^{17}\text{O}$ uses only components (1) and (2), because (3) is mass-dependent and does not affect $\Delta^{17}\text{O}$.

After SIMS analyses backscattered electron (BSE) images were collected of sputtered pits. Fifteen of 404 pits significantly overlapped surface imperfections and/or foreign phases (>20% of the pit); such analyses were rejected

due to an increased likelihood of erroneous $\delta^{18}\text{O}$ and $\delta^{17}\text{O}$ data.

3. RESULTS

Representative BSE images of chondrules are shown in [Fig. 2](#). BSE images of all chondrules, denoting SIMS pits and analysis numbers, are shown in [Appendix EA2](#). EMP data are compiled in [Appendix EA3](#). Individual oxygen isotope measurements are summarized in [Appendix EA4](#).

3.1. Chondrule petrography and mineralogy

Within the MET 00426,46 section essentially every chondrule/fragment was investigated ([Appendix EA2](#)), constituting 26 type I chondrules/fragments, and 3 type II chondrule fragments. Type I chondrules/fragments range from 200 μm to 2 mm in diameter, while type II chondrule fragments are 70–100 μm in size. Twenty-five type I chondrules/fragments are porphyritic; 3 are porphyritic olivine (PO; >80% modal olivine, relative to pyroxene) (e.g. [Fig. 2a](#)), 4 are porphyritic pyroxene (PP; <20% modal olivine) (e.g. [Fig. 2b](#)), and 18 are porphyritic olivine-pyroxene (POP; 20–80% modal olivine) (e.g. [Fig. 2c](#)) in texture. One type I chondrule has a barred olivine (BO) texture ([Fig. 2d](#)). Type II chondrule fragments are PO textured (e.g. [Fig. 2e](#) and [f](#)). Fifteen of 29 objects have a high degree of angularity along their outer periphery, leading to their classification as chondrule fragments (e.g. [Ebel et al., 2008](#)). One chondrule, M5, is irregular in shape ([Appendix EA2](#)). Admittedly, classification of chondrules as fragments, or as being irregularly-shaped, is somewhat subjective. Within each type I chondrule/fragment, olivine and low-Ca pyroxene compositions are spatially homogeneous, with typical Fo, En, and Wo variations of 0.2, 0.4 and 0.1, respectively (1SD). Chondrule fragment M3 (type I PP; [Fig. 2b](#)) exhibits the greatest spatial variability, as low-Ca pyroxenes vary by 1.6 and 1.2 (1SD) in En and Wo. Averaged olivine Fo contents among type I chondrules range from 96.7 to 99.2, and averaged low-Ca pyroxene En and Wo contents range from 91.4 to 98.1, and 0.4 to 3.0, respectively. Within the bounds of EMP analyses type II chondrule fragments exhibit greater Fo spatial variability, as M11, M15, and M25 have 1SD's of 0.8, 3.7, and 1.8, respectively ([Appendix EA3](#)). No high Fo content cores are present in their phenocrysts (e.g. [Fig. 2e, f](#)). Averaged Fo contents in M11, M15, and M25 are 53.4, 53.8, and 62.2, respectively.

The QUE 99177,49 section has 55 type I chondrules/fragments ([Appendix EA2](#)). No suitable type II chondrules/fragments were located. Nineteen of 55 were chosen for characterization based on (1) maximizing the range of constituent olivine/pyroxene Mg#’s; and (2) the presence of measurable anorthite for future ^{26}Al – ^{26}Mg isotope chronology by SIMS. Chosen chondrules/fragments are 400 μm to 3 mm in size. Of the 19 type I chondrules/fragments, 15 are POP (e.g. [Fig. 2h](#)) and 1 is a PO chondrule ([Fig. 2i](#)). The remaining three chondrules are layered/compound in texture; two consist of a BO core and a POP periphery ([Fig. 2j](#) and [k](#)), and one is a large POP chondrule containing

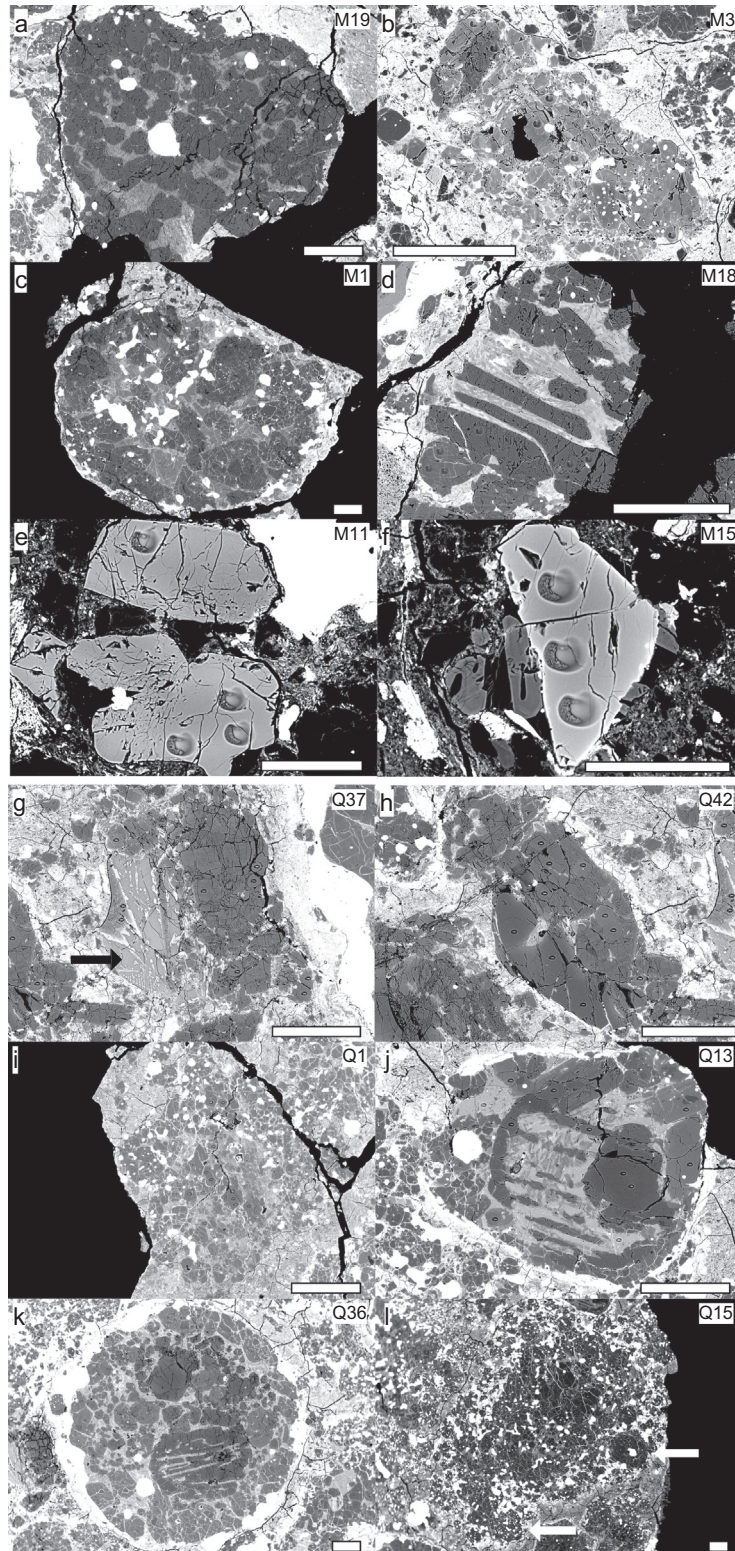


Fig. 2. Representative BSE images of chondrules from MET 00426 and QUE 99177. Scalebars are 200 μm , except for panels e and f, which are 50 μm . From MET 00426: (a) M19, a type I porphyritic olivine (PO) chondrule; (b) M3, a type I porphyritic pyroxene (PP) chondrule fragment; (c) M1, a type I porphyritic olivine-pyroxene (POP) chondrule; (d) M18, a type I barred olivine (BO) textured chondrule; (e and f) M11 and M15, type II PO chondrule fragments. From QUE 99177: (g) Q37, a type I POP chondrule fragment with glassy mesostasis (black arrow); (h) Q42, a type I POP chondrule fragment; (i) Q1, a type I PO chondrule; (j) Q13, a type I compound chondrule with BO and POP features; (k) Q36, a type I compound chondrule with BO and POP features; (l) Q15, a type I layered chondrule that is POP textured, with smaller chondrules along the outer periphery (white arrows). In many of the panels, the 15 μm pits from SIMS analyses are easily visible.

small chondrules along its periphery (Fig. 2l). Seven of 19 are classified as chondrule fragments, and four chondrules are irregularly shaped. Similar to MET 00426, multiple EMP analyses within QUE 99177 chondrules/fragments revealed spatially homogeneous olivines and low-Ca pyroxenes, with typical Fo, En, and Wo 1SD values of 0.2, 0.3, and 0.1, respectively. Chondrule fragment Q42 (POP; Fig. 2h) exhibits the greatest spatial variability, as olivine Fo contents vary by 1.1 (1SD) (Appendix EA3). Chondrule Q13, a compound chondrule, contains a large Fo_{99.3} phenocryst set in a Fo_{98.4} barred olivine texture (Fig. 2j). This phenocryst has features suggesting it may or may not have crystallized from the final chondrule melt (Appendix EA5). Averaged Fo contents among chondrules/fragments range from 95.7 to 99.2, and averaged chondrule low-Ca pyroxene En and Wo contents range from 94.2–98.1 and 0.4–3.0, respectively (Appendix EA3).

Chondrules from MET 00426 and QUE 99177 have similar accessory phases. All type I chondrules/fragments have Fe, Ni metal and the type II chondrule fragments have small amounts of Fe-sulfides, as determined by EDS. All measured chondrules/fragments have mesostasis; 43 of 48 have mesostasis with a heterogeneous texture, typically consisting of fine-to-coarse grained pyroxene and plagioclase (e.g. Fig. 3). Type II chondrule fragments M11, M15, and M25 have glassy mesostasis, with approximate SiO₂, Al₂O₃, FeO, MgO, CaO, and Na₂O contents of 60, 8 to 14, 13, 2 to 5, 0.5, and 8 to 12 wt.%, respectively, determined by EDS. Type I chondrule fragments M12 and Q37 also have glassy mesostasis (e.g. Fig. 2g), with approximate SiO₂, Al₂O₃, FeO, MgO, CaO, and Na₂O contents (by EDS) of 56, 24, 1, 3, 12, and 2.5 wt.%, respectively, in M12, and 68, 15, 4, 1.5, 6.5, and 3.5 wt.%, respectively, in Q37. No replacement phyllosilicates, commonly found in CR2 chondrule mesostasis (e.g. Weisberg et al., 1993; Krot et al., 2002a), were observed in the CR3 chondrules/fragments. As mesostasis regions are typically too small for a 15 μm SIMS spot analysis, and/or are heterogeneous and quench textured, we chose not to measure their oxygen isotopes. Accessory Ca-pyroxene and plagioclase are associated with mesostasis in type I chondrules; specifically, they exhibit overgrowth textures consistent with late-stage crystallization from the chondrule melt (e.g. Fig. 3). Regarding accessory pyroxenes, there are two distinct compositions: high-Ca pyroxene (En: 53.9–64.4; Wo: 32.9–44.7;

Appendix EA3), and pyroxene with an intermediate composition (En: 89.7–95.4; Wo: 3.5–8.4; Appendix EA3). Intermediate pyroxenes are more calcic than coexisting low-Ca pyroxenes, and are similar in composition to intermediate pyroxenes measured in type I Mokoia CV3 chondrules by Jones and Schilk (2009). Many intermediate pyroxenes are CaO-depleted relative to pigeonite, which is defined as Wo_{5–20}. Chondrule Q37 has laths of zoned accessory pyroxene overgrowths that are less calcic (Wo: 0.5–1.2) than typical intermediate pyroxenes, but are more calcic than coexisting low-Ca pyroxene (Wo: 0.3) (Appendix EA3). For this reason we refer to these as intermediate pyroxene, but they are also zoned in Al, Cr, Mn, and Ti (Appendix EA3). Anorthite contents of crystalline plagioclase (verified by optical microscopy) range from 72 to 92, using calculation methods from Beatty and Albee (1980).

3.2. Chondrule Mg#

In 36 of the type I chondrules, EMP measurements allow for comparing Mg#’s of coexisting olivine and low-Ca pyroxene. Per chondrule, 35 of 36 have coexisting olivines and low-Ca pyroxenes with Mg#’s that differ by one or less (Fig. 4). In chondrule Q5 olivine phenocrysts have slightly higher Mg#’s (98.3), relative to low-Ca pyroxenes (96.3; Fig. 4); this relationship is examined within the context of respective oxygen isotope measurements in section 4.1.

The similarity of coexisting olivine and pyroxene Mg#’s is a common occurrence in chondrules from chondrites that experienced minimal thermal metamorphism and aqueous alteration (Jones, 1994; Tachibana et al., 2003; Ushikubo et al., 2012; Tenner et al., 2013; Fig. 4). Based on this same occurrence in MET 00426 and QUE 99177 chondrules/fragments, and also stemming from the dominance of olivine and/or low-Ca pyroxene in chondrule silicate assemblages, we define the Mg# of a chondrule as the average of its constituent olivine and/or low-Ca pyroxene. This is the same definition employed by Ushikubo et al. (2012) and Tenner et al. (2013) for chondrules from Acfer 094 (ungr. C 3.00) and CO3.05 chondrites, respectively. Uncertainties in chondrule Mg# are defined as the range; specifically, we use the maxima and minima of measured olivine and/or low-Ca pyroxene Mg#’s per chondrule, and calculate their differences relative to the chondrule Mg#. By this

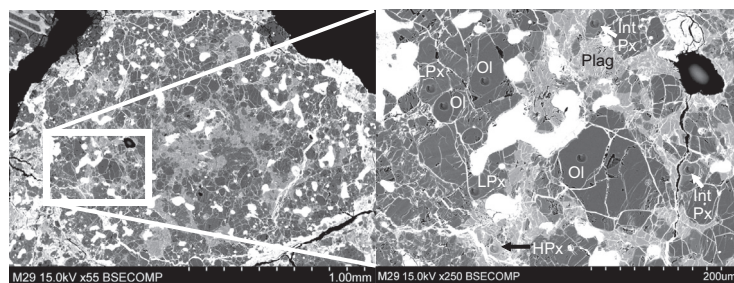


Fig. 3. BSE images of type I POP chondrule M29, illustrating typical textures of accessory high-Ca pyroxene, intermediate pyroxene, and plagioclase. Each accessory phase is associated with mesostasis in type I chondrules/fragments. SIMS pits are labeled according to mineral phase.

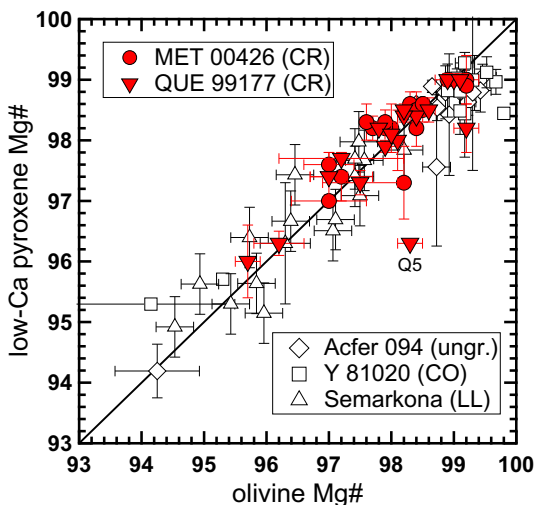


Fig. 4. Comparison of olivine and low-Ca pyroxene Mg#'s in chondrules from MET 00426 and QUE 99177, as well as comparisons of type I chondrules from Semarkona (LL3.0; Jones, 1994; Tachibana et al., 2003), Acfer 094 (ungr. C 3.00; Ushikubo et al., 2012), and Yamato 81020 (CO3.05; Tenner et al., 2013) chondrites. Each datum represents the averaged Mg# of olivine and low-Ca pyroxene that coexist within a single chondrule, showing 1SD uncertainties. The solid line represents a one to one relationship. Data from chondrule Q5 are examined within the context of respective oxygen isotope measurements in Section 4.1.

definition, greater uncertainties in chondrule Mg#, due either to slight spatial variability from igneous zoning (e.g. chondrule fragments M3 and Q42, described in 3.1) or differences in Mg#'s between constituent olivine and low-Ca pyroxene (e.g. chondrule Q5) are accounted for. This definition is also appropriate for the MET 00426 type II chondrule fragments, because larger spatial variabilities in their olivine compositions, likely due to igneous zoning, are accounted for. Chondrule Mg#'s are summarized in Table 1.

3.3. Oxygen isotope ratios

A total of 389 SIMS spot analyses of unknowns, collected in two sessions (one each for MET 00426 and QUE 99177 sections), were used to assess oxygen isotope systematics of chondrules (Appendix EA4). Regardless of which mineral phase was measured, data from each chondrule exhibit nearly indistinguishable oxygen isotope ratios and plot on the PCM line (e.g. Fig. 5a and b). Averaged chondrule $\delta^{18}\text{O}$, $\delta^{17}\text{O}$, and $\Delta^{17}\text{O}$ values typically have propagated uncertainties of 0.5‰, 0.4‰, and 0.3‰, respectively (Appendix EA4). Table 1 lists the minerals measured per chondrule, and the number of measurements per mineral. For a given chondrule, the homogeneity of oxygen isotopes among different minerals indicates each phase crystallized from the final chondrule melt, thus, defining the chondrules host oxygen isotope ratio. However, five type I chondrules, M2, Q1, Q15, Q42, and Q44, have SIMS measurements of olivine grains that do not match respective homogeneous chondrule data (e.g. Fig. 5b); their $\Delta^{17}\text{O}$ values are 1–2‰

lower when compared to respective host chondrule values (Fig. 5d). As such, these olivines are defined as relicts (Section 2.3). Their $\Delta^{17}\text{O}$ values (–3.2‰ to –5.8‰; Table 1) are within the range of host values measured in type I chondrules from this study and from other carbonaceous chondrites (Rudraswami et al., 2011; Libourel and Chaussidon, 2011; Ushikubo et al., 2012; Tenner et al., 2013; Schrader et al., 2013).

Averaged host chondrule oxygen isotope ratios are given in Table 1. On a three-oxygen isotope diagram, 37 of 48 averaged chondrule data overlap the PCM line if considering their uncertainties; the remaining chondrules plot within 0.8‰ of the PCM line (Fig. 6). Chondrule $\Delta^{17}\text{O}$ values nearly continuously range from –5.9‰ to +0.6‰ (e.g. Fig. 5d); specifically, type I chondrules have $\Delta^{17}\text{O}$ values between –5.9‰ and –0.8‰; type II chondrule fragments are comparatively ^{16}O -poor, with $\Delta^{17}\text{O}$ values of 0.2–0.6‰. Although type II chondrules from LL3 chondrites have similar $\Delta^{17}\text{O}$ values (e.g. Kita et al., 2010), the type II CR3 chondrule fragments are ~ 1 ‰ greater in $\delta^{18}\text{O}$.

4. DISCUSSION

4.1. Chondrule Mg# vs. $\Delta^{17}\text{O}$

Among the type I chondrules there is a well-defined correlation of increasing $\Delta^{17}\text{O}$, from –5.9‰ up to –0.8‰, with decreasing chondrule Mg#, from 99.2 to ~ 96 ; only chondrule Q37 (Mg#: 95.8; $\Delta^{17}\text{O}$: –3.3‰), significantly deviates from this relationship (Fig. 7). To the best of our knowledge, this is the first time such a continuous trend has been found among type I chondrules within a single carbonaceous chondrite group. In addition, four chondrules with Mg#'s ranging from 94 to 53 are ^{16}O -poor relative to Mg# > 96 chondrules, with $\Delta^{17}\text{O}$ values of –0.8‰ to 0.6‰.

In chondrule Q5, oxygen isotope ratios of coexisting olivine and low-Ca pyroxene are indistinguishable within analytical uncertainties (Appendix EA4), suggesting they represent the host chondrule value. However, the olivines in Q5 have comparatively higher Mg#'s than the low-Ca pyroxenes (Fig. 4; Appendix EA3). This could have occurred if the olivines crystallized at high temperatures where Fe condensation was incomplete, and if low-Ca pyroxenes crystallized at lower temperatures, where Fe condensation was more complete (e.g. Ebel and Grossman, 2000). Alternatively, the olivines could have crystallized under more reducing conditions than the low-Ca pyroxene, in such a manner that did not influence the oxygen isotope ratio of the chondrule melt. However, it cannot be ruled out that Q5 olivines instead have a relict origin, and formed in an oxygen isotope reservoir with the same value as the final chondrule melt. If so, the Mg# of low-Ca pyroxene in Q5, 96.3 ± 0.1 (Appendix EA3), would more closely approximate the chondrule Mg#, rather than the value we report in Table 1 (97.3 ± 1.1).

The observation that type I CR chondrules become increasingly ^{16}O -poor with decreasing Mg#, arguably trending towards the Mg#'s and oxygen isotope ratios of type II CR chondrules (e.g. Fig. 7), suggests precursors

Table 1
Oxygen isotope data for MET 00426 and QUE 99177 chondrules.

Chondrule ^a	Type, texture	n(ol, lpx, int. px, hpx, pl)	$\delta^{18}\text{O}$	unc.	$\delta^{17}\text{O}$	unc.	$\Delta^{17}\text{O}$	unc.	$\Delta^{17}\text{O}$ 2SD	Mg# ^b	+/- ^c
<i>MET 00426</i>											
M1	I, POP	4,5,0,4,0	1.9	0.5	-0.3	0.4	-1.4	0.3	0.5	97.0	0.5,0.6
M2	I, POP	3,3,1,0,0	1.0	0.8	-1.2	0.8	-1.6	0.3	0.6	97.9	0.5,0.3
	M2 relict ol	1,0,0,0,0	-1.3	0.3	-3.9	0.6	-3.2	0.6	n.a.	97.7	n.a.
M3 (f)	I, PP	0,7,0,0,0	2.7	0.4	0.5	0.3	-0.9	0.3	0.4	94.2	1.0,0.7
M4	I, POP & BO	1,4,0,0,0	-0.2	0.3	-2.7	0.3	-2.6	0.3	0.5	98.5	0.3,0.2
M5 (ir.)	I, POP	3,2,0,0,0	0.0	0.5	-2.9	0.3	-2.9	0.3	0.5	98.1	0.4,0.2
M6 (f)	I, POP	4,4,0,0,0	-2.3	0.4	-5.4	0.4	-4.2	0.2	0.6	99.0	0.1,0.1
M7 (f)	I, PP	0,4,0,0,0	3.1	0.5	0.8	0.5	-0.8	0.4	0.8	96.7	0.2,0.6
M8 (f)	I, POP	3,0,0,0,0	2.2	0.4	-0.6	0.7	-1.8	0.7	1.1	97.9	0.2,0.3
M9	I, POP	4,4,1,4,0	2.9	0.4	0.7	0.4	-0.9	0.3	0.5	97.3	0.5,0.6
M10	I, POP	4,4,0,0,0	1.1	0.5	-1.8	0.4	-2.3	0.2	0.4	97.3	0.5,0.8
M11 (f)	II, PO	4,0,0,0,0	5.4	0.3	3.0	0.5	0.2	0.5	0.3	53.4	0.9,0.8
M12 (f)	I, POP	4,4,1,3,0	-5.3	0.5	-8.3	0.4	-5.6	0.3	0.5	99.1	0.3,0.5
M13 (f)	I, POP	1,4,0,0,0	-0.3	0.3	-2.6	0.3	-2.4	0.2	0.4	98.6	0.2,0.1
M14 (f)	I, POP	3,4,0,2,0	0.4	0.6	-1.9	0.5	-2.1	0.3	0.7	98.0	0.6,0.4
M15 (f)	II, PO	3,0,0,0,0	5.6	0.3	3.5	0.6	0.6	0.6	0.6	53.8	3.3,4.1
M16	I, POP	4,3,0,1,0	1.0	0.5	-1.8	0.3	-2.3	0.3	0.7	97.8	0.5,1.0
M17	I, POP	4,4,0,0,0	0.6	0.4	-2.1	0.3	-2.4	0.2	0.5	98.3	0.2,0.6
M18	I, BO	4,3,0,0,0	-5.2	0.5	-8.1	0.6	-5.3	0.4	1.0	99.0	0.1,0.1
M19	I, PO	8,0,0,0,0	1.3	0.3	-1.2	0.2	-1.9	0.2	0.6	98.4	0.1,0.2
M20	I, POP	1,2,0,1,0	-2.2	1.0	-4.4	0.6	-3.2	0.5	0.2	98.4	0.3,0.2
M21	I, POP	3,4,3,0,0	1.1	0.5	-1.0	0.3	-1.6	0.2	0.5	98.1	0.3,0.2
M22 (f)	I, PO	8,0,0,0,0	-5.5	0.3	-8.8	0.3	-5.9	0.2	0.4	99.1	0.2,0.1
M23	I, POP	6,0,2,0,0	-3.5	0.7	-6.5	0.4	-4.7	0.2	0.4	99.2	0.1,0.1
M24 (f)	I, POP	2,3,2,0,0	0.2	0.5	-2.0	0.4	-2.2	0.2	0.3	98.5	0.2,0.3
M25 (f)	II, PO	3,0,0,0,0	5.7	0.4	3.3	0.6	0.3	0.6	0.3	62.2	2.1,1.1
M26 (f)	I, PO	6,0,0,0,0	0.5	0.5	-2.7	0.3	-2.9	0.2	0.5	98.4	0.1,0.1
M27 (f)	I, PP	0,4,0,0,0	1.2	0.5	-1.1	0.3	-1.8	0.2	0.2	97.8	0.4,0.5
M28 (f)	I, POP	4,4,0,0,0	0.9	0.4	-1.5	0.4	-2.0	0.3	0.7	98.1	0.4,0.3
M29	I, POP	4,4,4,1,0	-0.3	0.4	-2.6	0.3	-2.4	0.3	0.7	98.6	0.2,0.2
<i>QUE 99177</i>											
Q1	I, PO	6,0,2,0,0	-1.4	0.4	-4.8	0.4	-4.1	0.3	0.8	98.6	0.1,0.2
	Q1 relict ol	1,0,0,0,0	-4.7	0.6	-8.2	0.4	-5.8	0.5	n.a.	98.4	n.a.
Q4 (f)	I, POP	4,4,0,1,0	2.1	0.5	-1.0	0.3	-2.1	0.2	0.4	96.3	0.4,0.6
Q5	I, POP	4,4,0,0,0	3.1	0.4	0.3	0.2	-1.3	0.2	0.2	97.3	1.2,1.1
Q7 (ir.)	I, POP	5,3,0,0,2	-2.9	0.5	-6.8	0.3	-5.2	0.3	0.5	99.0	0.2,0.1
Q13	I, compound	3,4,0,0,2	1.1	0.4	-1.4	0.4	-1.9	0.3	0.6	98.4	0.2,0.2
Q15	I, layered	4,5,0,1,1	-0.3	0.4	-3.0	0.3	-2.8	0.2	0.5	98.6	0.1,0.3
	Q15 relict ol	1,0,0,0,0	-5.2	0.4	-8.4	0.6	-5.7	0.5	n.a.	98.7	n.a.
Q16 (f)	I, POP	4,4,1,0,1	-3.2	0.4	-6.7	0.3	-5.0	0.3	0.6	99.0	0.2,0.3
Q19 (f)	I, POP	4,4,0,0,0	-3.2	0.4	-6.5	0.5	-4.9	0.3	0.9	98.7	0.7,0.8
Q24 (ir.)	I, POP	4,4,0,0,1	1.7	0.5	-1.1	0.3	-2.0	0.2	0.5	98.0	0.3,0.3
Q35 (ir.)	I, POP	4,2,1,0,1	2.3	0.5	-0.9	0.4	-2.1	0.3	0.8	98.3	0.2,0.3
Q36	I, compound	7,7,0,0,0	2.3	0.4	-0.5	0.3	-1.7	0.3	0.3	97.4	0.7,0.9
Q37 (f)	I, POP	3,3,3,0,0	-0.7	0.4	-3.7	0.3	-3.3	0.2	0.4	95.8	0.8,0.4
Q38 (f)	I, POP	3,4,0,0,1	-4.0	0.7	-7.4	0.3	-5.3	0.3	0.8	99.0	0.1,0.2
Q42 (f)	I, POP	6,3,0,0,0	0.5	0.5	-2.3	0.4	-2.6	0.3	0.7	97.5	0.8,1.5
	Q42 relict ol	1,0,0,0,0	-4.1	0.4	-7.5	0.4	-5.4	0.4	n.a.	96.5	n.a.
Q43	I, POP	6,2,4,0,0	1.1	0.4	-1.8	0.3	-2.4	0.2	0.5	97.2	0.4,0.6
Q44	I, POP	3,4,0,1,1	0.7	0.4	-2.0	0.3	-2.4	0.2	0.5	98.3	0.2,0.2
	Q44 relict ol	1,0,0,0,0	-1.5	0.2	-5.1	0.4	-4.4	0.4	n.a.	98.1	n.a.
Q47 (ir.)	I, POP	4,3,1,0,1	-0.3	0.5	-2.7	0.4	-2.6	0.2	0.4	97.9	0.1,0.1
Q51	I, POP	3,3,0,0,0	0.8	0.5	-1.6	0.4	-2.0	0.3	0.7	98.1	0.3,0.6
Q53 (f)	I, POP	4,4,2,0,0	1.1	0.4	-1.6	0.3	-2.2	0.2	0.4	98.1	0.3,0.2

^a (f) = chondrule fragment; (ir.) = irregularly shaped chondrule. Discussions in Zanda et al. (2002) and Ebel et al. (2008) were used as guides to distinguish chondrule fragments from irregularly shaped chondrules.

^b Chondrule Mg# = molar% MgO/(MgO + FeO) of constituent olivine and/or low-Ca pyroxene.

^c Uncertainties represent the range in measured Mg#'s of constituent olivine and/or low-Ca pyroxenes in chondrules.

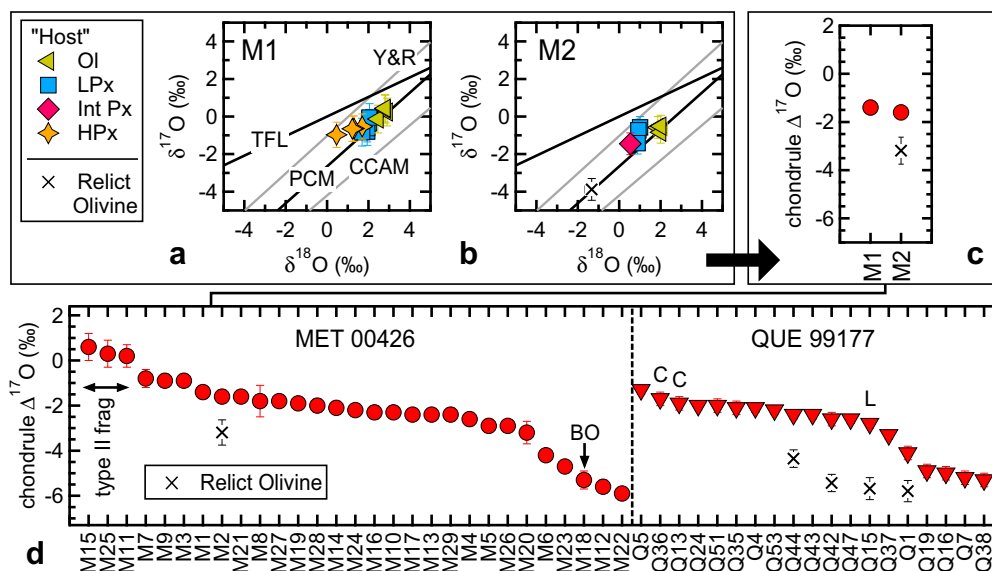


Fig. 5. (a) oxygen three-isotope diagram of SIMS data from chondrule M1. Measurements from multiple phases (OI: olivine; LPx: low-Ca pyroxene; Int Px: intermediate pyroxene; HPx: high-Ca pyroxene) yield nearly homogeneous data, indicating they crystallized from the final chondrule melt and represent the “host” chondrule oxygen isotope ratio. Shown for comparison are the primitive chondrule mineral (PCM; Ushikubo et al., 2012), carbonaceous chondrite anhydrous mineral (CCAM; Clayton et al., 1977, Young and Russell (1998), and terrestrial fractionation lines. Uncertainties are the external reproducibility of bracketing San Carlos olivine measurements. (b) oxygen three-isotope diagram of SIMS data from chondrule M2. One measurement from an olivine grain exceeds the 3SD of the average $\Delta^{17}\text{O}$ ($=\delta^{17}\text{O}-0.52 \times \delta^{18}\text{O}$) of the other 6 measurements; this criterion defines the olivine as a “relict” grain, meaning it derived its oxygen isotope ratio from a previous generation of chondrule melting/crystallization. (c) $\Delta^{17}\text{O}$ values of chondrule M1 and M2, taken as the average of the “host” mineral data shown in (a) and (b). Relict grains are excluded when determining chondrule $\Delta^{17}\text{O}$. Propagated 2SE uncertainties are smaller than the symbols. (d) Averaged $\Delta^{17}\text{O}$ values of all MET 00426 (red circles) and QUE 99177 (inverted red triangles) chondrules/fragments from this study. Uncertainties are the propagated 2SE of the “host” mineral data per chondrule/fragment. Unless otherwise noted, chondrules/fragments are type I. BO: type I barred olivine texture; C: type I compound chondrule; L: type I layered chondrule. Also shown are data from relict olivine grains. (For interpretation of the references to colour in this figure legend, the reader is referred to the web version of this article.)

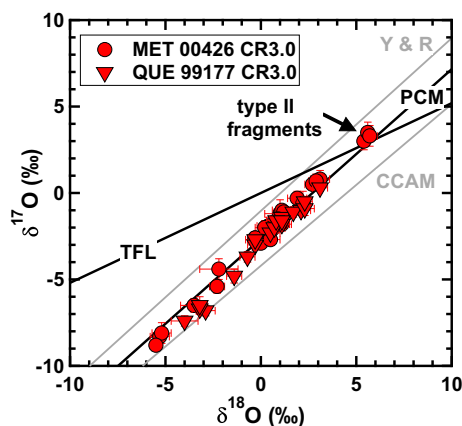


Fig. 6. Oxygen three-isotope diagram illustrating values of chondrules from MET 00426 (red circles) and QUE 99177 (inverted red triangles). Each datum is the averaged $\delta^{18}\text{O}$ and $\delta^{17}\text{O}$ value of a chondrule. Uncertainties are propagated 2SE. Shown are the primitive chondrule mineral (PCM; Ushikubo et al., 2012), carbonaceous chondrite anhydrous mineral (CCAM; Clayton et al., 1977, Young and Russell (1998), and the terrestrial fractionation lines. (For interpretation of the references to colour in this figure legend, the reader is referred to the web version of this article.)

were predominantly influenced by the following: (1) a ^{16}O -poor oxidizing agent, and/or (2) a ^{16}O -rich reducing agent. Regarding the former, H_2O ice in the Solar nebula may have been a contributor, as suggested by Connolly and Huss (2010), because it is relatively ^{16}O -poor (e.g. Sakamoto et al., 2007; Yurimoto et al., 2008; Fig. 1). In addition, carbonaceous chondrites likely accreted farther from the Sun than enstatite and ordinary chondrites (Rubin and Wasson, 1995), where there could have been abundant H_2O ice (Cuzzi and Zahnle, 2004). Regarding the latter, gas of a Solar composition may have played a role, as it imposes highly reducing conditions (e.g. Grossman et al., 2008), and was probably ^{16}O -rich (e.g. McKeegan et al., 2011; Fig. 1). It is also possible that reduced ^{16}O -poor organic matter (e.g. Hashizume et al., 2011; Fig. 1) was a contributor, but addition of such carbon-rich material would tend to form chondrules with higher Mg#’s (e.g. Connolly et al., 1994) and higher $\Delta^{17}\text{O}$ values; this relationship is opposite of the trend in Fig. 7. As such, one might expect the influence of organic matter on the CR3 chondrule Mg# and oxygen isotope relationship to be rather limited.

Within chondrule precursors abundances of H_2O , Solar gas, and organic material were likely intimately related to the degree of dust enrichment, which has long been

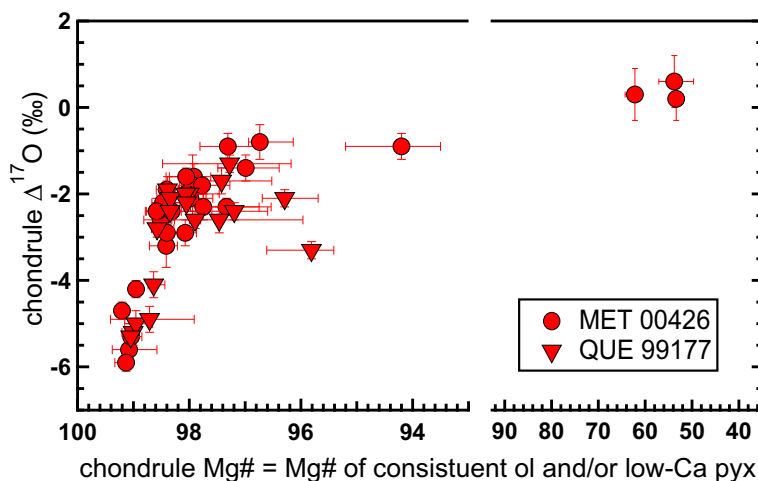


Fig. 7. MET 00426 (red circles) and QUE 99177 (red inverted triangles) chondrule Mg#'s versus $\Delta^{17}\text{O}$ values. Each datum represents the Mg# and averaged $\Delta^{17}\text{O}$ value of a single chondrule. Chondrule Mg# uncertainty represents the range of measured values, while uncertainties in $\Delta^{17}\text{O}$ are the propagated 2SE. (For interpretation of the references to colour in this figure legend, the reader is referred to the web version of this article.)

considered a necessary condition to form chondrules (e.g. Wood, 1967), and is one of the most plausible mechanisms for controlling $f\text{O}_2$ during chondrule formation (e.g. Ebel and Grossman, 2000); critically, we can use the Mg# and oxygen isotope relationship of CR3 chondrules to quantify each of these parameters. In the following sections we use several aspects of existing equilibrium condensation models and a simple oxygen isotope mass balance to determine if the CR3 chondrule Mg# and oxygen isotope relationship can be explained by mixing of various endmember chondrule precursor components.

4.2. Assessing the influence of the precursor assemblage on redox conditions during chondrule formation

In order to evaluate redox conditions during CR chondrule formation, influences imposed by compositional changes of the precursor assemblage must be constrained. Dust enrichment is defined as adding a specified amount of a solid component, often CI chondritic in composition, to gas of a Solar composition (Ebel and Grossman, 2000). At an enrichment factor of n , the composition of an assemblage is obtained by adding $(n - 1)$ units of dust to Solar gas. Atomic abundances of Solar gas and dust are normalized to 10^6 atoms of Si. Shown in Table 2, the net effect of dust enrichment is oxidation of the chondrule-forming environment. For instance, Ebel and Grossman (2000) calculate that precursors enriched in CI dust by $100\times$, $500\times$, and $1000\times$ (total pressure, P^{tot} : 10^{-3} atm) yield increases in $f\text{O}_2$ by ~ 3 , 4.5, and 5 log units, respectively, when compared to gas of a Solar composition. This effect is temperature independent; Fig. 4 from Ebel and Grossman (2000) illustrates $\log f\text{O}_2$ versus temperature curves of precursor assemblages that are concentric with one another, and also to the iron-wüstite buffer, from 1200 to 2400 K.

In addition to dust enrichment, enhancement of chondrule precursors in H_2O ice may have occurred by transport

of icy materials to the inner regions of the protoplanetary disk (Ciesla and Cuzzi, 2006). Such a process would have contributed to oxidizing the chondrule-forming environment. For example, Grossman et al. (2008) predict that “icy” Solar gas (which they define as $10\times$ relative H_2O abundance) yields an oxygen fugacity ~ 2 log units higher than nominal Solar gas at a P^{tot} of 10^{-3} atm. (Table 2). Further, Fedkin and Grossman (2006) calculate that $125\times$ “icy” CI dust (which they define as 1 part H_2O per 10 parts Orgueil by weight) is ~ 0.3 log units more oxidizing than nominal $125\times$ CI dust at a P^{tot} of 10^{-3} bar. Similar to Ebel and Grossman (2000), models from Fedkin and Grossman (2006) and Grossman et al. (2008) show the effect of increased $f\text{O}_2$ by ice enhancement does not change, relative to the IW buffer, from 1450 to 2000 K.

Along with H_2O , chondrule precursors might have a significant amount of carbon (Table 2), which is a reducing agent. Therefore, the influence of carbon on $f\text{O}_2$ must be taken into account. We assess this below.

The oxygen fugacity imposed by a precursor assemblage is strongly controlled by the abundances of H, O, and C (e.g. Eq. 24 from Grossman et al., 2008), which are directly related to the degree of enrichment in dust, H_2O , and organic material. As H/O and C/O ratios of a given assemblage decrease, the chondrule-forming environment becomes more oxidized (Table 2); these relationships can be used to estimate $f\text{O}_2$ during chondrule formation, as shown in Fig. 8a and b. Here, we note that we have chosen to gather data and perform calculations at a reference temperature of 1480 K. This temperature is chosen because under equilibrium conditions (1) low dust enrichments at 1480 K predict a silicate phase assemblage of melt, olivine, Ca-poor pyroxene, and minor amounts of Ca-rich pyroxene and feldspar (e.g. Fig. 6d from Ebel and Grossman, 2000), which matches the phase assemblage in type I chondrules (e.g. Fig. 2); (2) higher dust enrichments at 1480 K predict a silicate phase assemblage dominated by melt and olivine (e.g. Fig. 7d from Ebel and Grossman, 2000), which

Table 2

Atomic abundances of Solar gas and CI dust; estimated imposed oxygen fugacities at 1480 K and P^{tot} : 10^{-3} atm or 10^{-3} bar, taken from [Ebel and Grossman \(2000\)](#) and [Grossman et al. \(2008\)](#).

	Solar ^{AP}	Solar ^{A&G}	Icy Solar ^a	CI dust ^{A&G}	100× CI ^b	500× CI ^b	1000× CI ^b
H	2.79×10^{10}	2.79×10^{10}	2.80×10^{10}	5.28×10^6	2.84×10^{10}	3.05×10^{10}	3.32×10^{10}
He	2.72×10^9	2.72×10^9	2.72×10^9	2.72×10^9	2.72×10^9	2.72×10^9	2.72×10^9
O	1.37×10^7	2.38×10^7	6.62×10^7	7.63×10^6	7.79×10^8	3.83×10^9	7.65×10^9
C	6.85×10^6	1.01×10^7	6.85×10^6	7.56×10^5	8.49×10^7	3.87×10^8	7.65×10^8
N	3.13×10^6	3.13×10^6	3.13×10^6	5.98×10^4	9.05×10^6	3.30×10^7	6.29×10^7
Mg	1.07×10^6	1.07×10^6	1.07×10^6	1.07×10^6	1.07×10^8	5.35×10^8	1.07×10^9
Si	1.00×10^6	1.00×10^6	1.00×10^6	1.00×10^6	1.00×10^8	5.00×10^8	1.00×10^9
Fe	9.00×10^5	9.00×10^5	9.00×10^5	9.00×10^5	9.00×10^7	4.50×10^8	9.00×10^8
S	4.46×10^5	5.15×10^5	4.46×10^5	5.15×10^5	5.15×10^7	2.58×10^8	5.15×10^8
Al	8.49×10^4	8.49×10^4	8.49×10^4	8.49×10^4	8.49×10^6	4.25×10^7	8.49×10^7
Ca	6.11×10^4	6.11×10^4	6.11×10^4	6.11×10^4	6.11×10^6	3.06×10^7	6.11×10^7
Na	5.74×10^4	5.74×10^4	5.74×10^4	5.74×10^4	5.74×10^6	2.87×10^7	5.74×10^7
Ni	4.93×10^4	4.93×10^4	4.93×10^4	4.93×10^4	4.93×10^6	2.47×10^7	4.93×10^7
Cr	1.35×10^4	1.35×10^4	1.35×10^4	1.35×10^4	1.35×10^6	6.75×10^6	1.35×10^7
P	1.04×10^4	1.04×10^4	1.04×10^4	1.04×10^4	1.04×10^6	5.20×10^6	1.04×10^7
Mn	9.55×10^3	9.55×10^3	9.55×10^3	9.55×10^3	9.55×10^5	4.78×10^6	9.55×10^6
K	3.77×10^3	3.77×10^3	3.77×10^3	3.77×10^3	3.77×10^5	1.89×10^6	3.77×10^6
Ti	2.40×10^3	2.40×10^3	2.40×10^3	2.40×10^3	2.40×10^5	1.20×10^6	2.40×10^6
Co	2.25×10^3	2.25×10^3	2.25×10^3	2.25×10^3	2.25×10^5	1.13×10^6	2.25×10^6
H/O	2041	1172	423	0.69	36.48	7.97	4.34
C/O	0.50	0.42	0.10	0.10	0.11	0.10	0.10
$\log f_{\text{O}_2} - \log \text{IW}$	-6.8 ^c	-6.1 ^d	-4.8 ^c		-3.1 ^d	-1.8 ^d	-1.3 ^d

*Solar gas and dust compositions are normalized to 10^6 atoms of Si. AP: [Allende Prieto and Lambert \(2001, 2002\)](#). A&G: [Anders and Grevesse \(1989\)](#).

^a Composition taken from [Grossman et al. \(2008\)](#). H₂O is added relative to the Solar gas composition from [Allende Prieto and Lambert \(2001, 2002\)](#).

^b Composition is calculated by adding $(n - 1)$ units of specified CI dust to the Solar gas composition from [Anders and Grevesse \(1989\)](#).

^c f_{O_2} determined from [Fig. 5](#) of [Grossman et al. \(2008\)](#).

^d f_{O_2} determined from [Fig. 4](#) of [Ebel and Grossman \(2000\)](#).

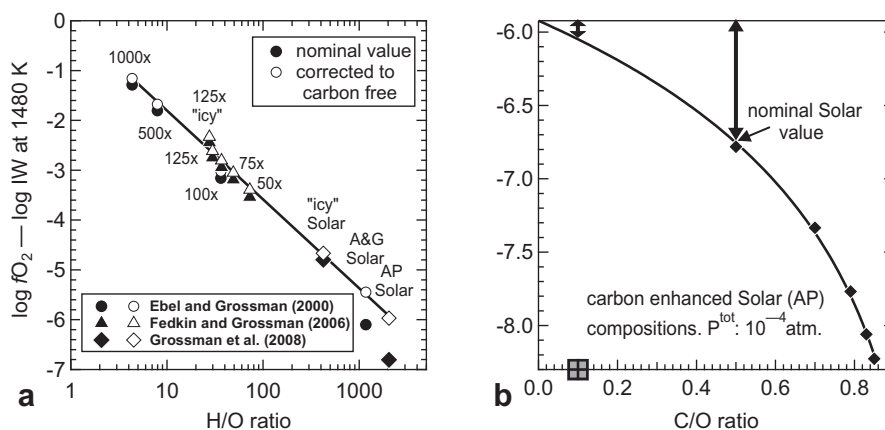


Fig. 8. (a) H/O versus f_{O_2} of systems enriched in CI dust at 1480 K and P^{tot} : 10^{-3} atm. or 10^{-3} bar. Data from [Ebel and Grossman \(2000\)](#) use the Solar gas composition from [Anders and Grevesse \(1989\)](#), while data from [Fedkin and Grossman \(2006\)](#) and [Grossman et al. \(2008\)](#) use the Solar gas composition from [Allende Prieto and Lambert \(2001, 2002\)](#). “Icy” Solar gas has 10× the amount of H₂O, by weight, relative to the nominal composition. The 125× “icy” CI dust enriched composition employs dust that consists of 1 part H₂O to 10 parts Orgueil by weight. (b) C/O versus oxygen fugacity of Solar gas from [Grossman et al. \(2008\)](#) at 1480 K and P^{tot} : 10^{-4} atm. Data fit: $\log f_{\text{O}_2} - \log \text{IW} = 1.2007 \times \ln(1 - \text{C/O}) - 5.9225$; $r^2 = 0.998$. Using this fit, imposed oxygen fugacities of assemblages can be corrected to carbon-free systems (i.e. C/O: 0), represented by vertical arrows. As dust enriched systems have low C/O ratios (e.g. [Table 2](#)), represented by the crossed gray box on the x-axis, the estimated correction in f_{O_2} is small. Open symbols in (a) illustrate data that are corrected to carbon-free (fit: $\log f_{\text{O}_2} - \log \text{IW} = -0.7740 \times \ln(\text{H/O}) - 0.0217$; $r^2 = 0.994$).

matches that of type II chondrules (e.g. [Fig. 2e](#) and [f](#)); and (3) greater than 98% of Fe is condensed at dust enrichments exceeding 100× at 1480 K (e.g. [Fig. 8a](#) and [b](#) from [Ebel and](#)

[Grossman, 2000](#)); this condition is likely necessary in order to explain the abundance of Fe, Ni metal in type I chondrules, as well as the amount of FeO in type II chondrules

(e.g. Fig. 2). Although the reference temperature is substantially lower than experimentally determined chondrule-forming conditions (i.e. 1720–1970 K; Hewins and Radomsky, 1990), predicted $\log f_{\text{O}_2} - \log \text{IW}$ values at 1480 K should be similar to those at higher temperatures, based on the aforementioned concentric $\log f_{\text{O}_2}$ versus T behavior of assemblages predicted by models.

Fig. 8a compares CI dust enriched systems from several studies. Although datasets differ with respect to the composition of Solar gas, or with respect to enhancement in ice, a well-defined trend of H/O versus $\log f_{\text{O}_2} - \log \text{IW}$ is produced. To account for the influence of carbon we apply a correction based on C/O versus f_{O_2} data from Grossman et al. (2008) from a system of Solar gas at 1480 K and a P^{tot} of 10^{-4} atm. (Fig. 8b), empirically fit by:

$$\log f_{\text{O}_2} - \log \text{IW} = 1.2007 \times \ln(1 - \text{C/O}) - 5.9225 \quad (1)$$

For CI dust enriched assemblages, which have C/O ratios of ~ 0.10 (Table 2), the correction is small; Eq. (1) predicts that a carbon-free system is only 0.13 log units higher in f_{O_2} ; however, the uncertainty of the correction is probably large for dust enriched assemblages, as their low C/O ratios represent a significant extrapolation from the Solar gas data used to produce Eq. (1) (e.g. Fig. 8b). Nonetheless, data from Fig. 8a are corrected to carbon-free systems using the “slope” from Eq. (1). Doing so allows for isolating the influence of an assemblage’s H/O ratio on f_{O_2} (open symbols; Fig. 8a), empirically fit by:

$$\log f_{\text{O}_2} - \log \text{IW} = -0.7740 \times \ln(\text{H/O}) - 0.0217 \quad (2)$$

By combining Eqs. (1) and (2) the oxygen fugacity imposed by a solid precursor at a specified dust enrichment factor and/or ice enhancement factor can be quantified:

$$\log f_{\text{O}_2} - \log \text{IW} = -0.7740 \times \ln(\text{H/O}) - 0.0217 + 1.2007 \times \ln(1 - \text{C/O}) \quad (3)$$

For simplicity, only changes in carbon contents of precursors that are directly tied to dust enrichment and ice enhancement are considered in the following models.

4.3. Estimating chondrule Mg# as a function of oxygen fugacity imposed by the precursor assemblage

Applying high-temperature equilibrium calculations, including MELTS (Ghiorso and Sack, 1995) and VAPORS (Ebel et al., 1999), Ebel and Grossman (2000) determined fayalite contents of olivine at specific CI dust enrichment factors. Using their data, we assume the Mg# of a chondrule is directly related to the olivine fayalite content (Section 3.2), and calculate the oxygen fugacity imposed by each dust enriched composition (Eq. (3)), which yields the following empirical fit at 1480 K (Fig. 9):

$$\text{chondrule Mg\#} = 100 - \exp(([\log f_{\text{O}_2} - \log \text{IW}] + 3.444)/0.6649) \quad (4)$$

By combining Eqs. (3) and (4) the redox conditions of the CR chondrule-forming environment can be evaluated. For example, type I chondrule Mg#'s (99.2–96; Fig. 7) indicate formation 2.5–3.6 log units below the IW buffer. In contrast, the type II chondrule fragments (Mg# 53–63; Fig. 7) formed under considerably more oxidizing conditions ($\log f_{\text{O}_2} - \log \text{IW}$: ~ -1). In terms of CI dust enrichment these results would suggest type I chondrules formed under 200 \times , while the type II chondrule fragments significantly exceeded 1000 \times (Fig. 9); however, as discussed later, these estimates can change if the dust composition deviates from that of CI dust, particularly with respect to the abundance of H₂O.

4.4. Estimating chondrule oxygen isotope ratios as a function of the precursor assemblage

In addition to controlling f_{O_2} , the degree of enrichments in dust, H₂O, and organic material likely dictated

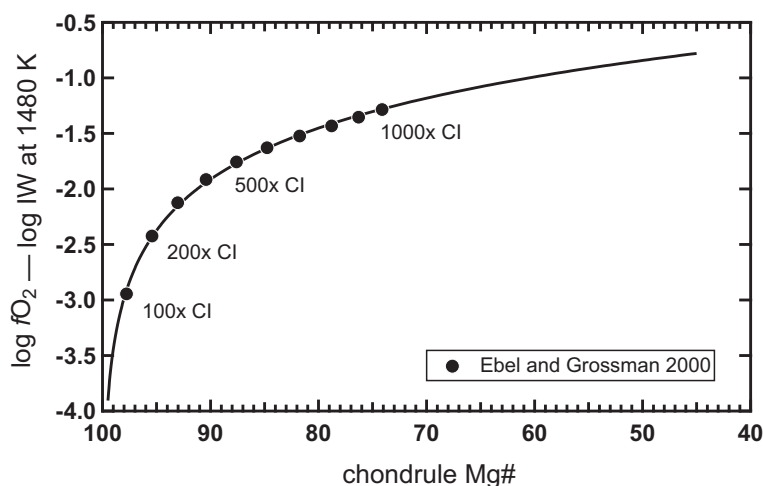


Fig. 9. Chondrule Mg# versus f_{O_2} at 1480 K and P^{tot} : 10^{-3} atm. Data are taken from Fig. 8a from Ebel and Grossman (2000). From their data, mole fractions of fayalite are converted to chondrule Mg# ($=100 - [X_{\text{Fa}} \times 100]$), which is appropriate based on definitions outlined in Section 3.2. CI dust enrichment factors are converted to imposed f_{O_2} values by determining H/O and C/O ratios for each assemblage (e.g. Table 2), where the composition of Solar gas is that from Anders and Grevesse (1989), and applying Eq. (3). Data fit: $\text{chondrule Mg\#} = 100 - \exp(([\log f_{\text{O}_2} - \log \text{IW}] + 3.444)/0.6649)$; r^2 : 0.999.

CR chondrule oxygen isotope ratios, as it is plausible to expect that chondrule precursors had multiple sources of oxygen isotopes with distinct ratios (e.g. Fig. 1). Therefore, the oxygen isotope ratio of a chondrule likely represents a mass balance involving the fractions of oxygen from each source and their respective oxygen isotope ratios. This concept can be used to determine the influence of various precursor enrichments on chondrule oxygen isotope ratios.

As an initial step we consider that chondrule precursors had four primary sources of oxygen isotopes, (1) Solar gas; (2) the silicate portion of the dust; (3) organic material in the dust; and (4) H₂O ice in the dust:

$$\begin{aligned} \text{chondrule } \Delta^{17}\text{O} = & (\text{frac. O}_{\text{Solar gas}} \times \Delta^{17}\text{O}_{\text{Solar gas}}) \\ & + (\text{frac. O}_{\text{silicate in dust}} \times \Delta^{17}\text{O}_{\text{silicate in dust}}) \\ & + (\text{frac. O}_{\text{organics in dust}} \times \Delta^{17}\text{O}_{\text{organics in dust}}) \\ & + (\text{frac. O}_{\text{H}_2\text{O in dust}} \times \Delta^{17}\text{O}_{\text{H}_2\text{O in dust}}) \quad (5) \end{aligned}$$

We use $\Delta^{17}\text{O}$ for simplicity in Eq. (5). It is implied $\delta^{17}\text{O}$ and $\delta^{18}\text{O}$ values of precursor components were on the PCM line, based on CR3 chondrule signatures (Fig. 6).

As a second step, the atomic abundances of oxygen from each source (given relative to 10^6 atoms of Si) must be established. For Solar gas we use the oxygen abundance from Allende Prieto and Lambert (2001, 2002), which is 1.367×10^7 atoms (Table 2). For sources in the dust, we assume a CI composition (Table 2), and assign oxygen to each component. For silicate in the dust, we calculate an abundance of 3.350×10^6 atoms (43.9% of oxygen in the dust; Table 3), solved by using the atomic abundances of Mg, Si, Al, Ca, Na, Cr, P, Mn, K, and Ti in CI dust (Table 2), and assigning oxygen to each as the following: MgO, SiO₂, Al₂O₃, CaO, Na₂O, Cr₂O₃, P₂O₅, MnO, K₂O, and TiO₂. We assume Fe, S, Ni, and Co in the dust existed as metal and sulfide at ambient conditions. For organic material we use the atomic abundance of carbon in CI dust (Table 2), and employ a C/O ratio of 5, which is that measured in IOM from Orgueil (CI) and Murchison (CM) chondrites (Binet et al., 2002; Remusat et al., 2007; for reference, these studies predict that IOM comprises 75–90% of the total carbon in the chondrites). This amounts to 1.512×10^5 atoms, or 2.0% of oxygen in the dust (Table 3). The remaining 54.1% of oxygen in the dust, 4.129×10^6 atoms, is assigned to H₂O ice (Table 3). By doing so, however, the necessary amount of hydrogen to make H₂O in the dust, 8.258×10^6 atoms (per 10^6 atoms of Si), is greater than the amount measured in CI chondrites, 5.28×10^6 atoms (Table 2). This discrepancy could represent a difference in how we assigned oxygen in model CI dust versus its actual association in CI chondrites. For instance, CI chondrites have oxidized Fe, while it is not expected that FeO was a primary condensate in the Solar nebula (Grossman et al., 2012); therefore, we choose to use the higher estimate for H instead of the measured value in CI chondrites (Table 3). We note that enrichment in this “modified” CI dust yields more reducing conditions (Eq. (3)), which predicts chond-

rules with marginally higher Mg#’s when compared to enrichment in nominal CI dust (Mg#’s at 100×: 97.9 vs. 97.9; 500×: 88.0 vs. 87.4; 1000×: 76.7 vs. 74.3, respectively; Eq. (4)).

As a final step, the oxygen isotope ratios of each source in the mass balance must be defined. For Solar gas, we use the estimated bulk Solar System value ($\Delta^{17}\text{O}$: -28.4‰), based on measurements of Solar wind by McKeegan et al. (2011). For the silicate in the dust we consider its oxygen isotope ratio is probably similar to the most ¹⁶O-rich high Mg# chondrule measured, and that addition of ¹⁶O-poor H₂O ice to the silicate contributed to forming chondrules with lower Mg#’s and higher $\Delta^{17}\text{O}$ values. Therefore, we assign a $\Delta^{17}\text{O}$ of -5.9‰ , which is the value of Mg# 99.1 chondrule fragment M22 (Table 1). For organic material in the dust, we use the average oxygen isotope composition measured by Hashizume et al. (2011) from the CR2 chondrite Yamato 793495, which has a $\Delta^{17}\text{O}$ value of 11.3‰ . For H₂O ice in the dust we calculate $\Delta^{17}\text{O}$; we use Eq. (5), and take advantage of the strong likelihood that type II (Mg# < 90) chondrules formed in highly dust-enriched environments (e.g. Fig. 9), where it can be assumed the oxygen isotope contribution from Solar gas is negligible (e.g. Table 3). Using (1) the average $\Delta^{17}\text{O}$ value of the three measured type II CR3 chondrule fragments (0.4‰ ; Table 1); (2) the fractions of atomic oxygen from the silicate, organic material, and ice in CI dust (0.439, 0.020, and 0.541, respectively; Table 3); and (3) the assigned $\Delta^{17}\text{O}$ values of organic and silicate components of the dust, Eq. (5) predicts that H₂O ice in CR3 chondrule precursors has a $\Delta^{17}\text{O}$ value of $+5.1\text{‰}$.

4.4.1. Efficiency of oxygen isotope exchange between ambient gas and chondrule melt

During chondrule formation, volatile species in solid precursors vaporized and mixed with Solar gas. The collective ambient gas then exchanged oxygen isotopes with the chondrule melt as the chondrule heated and cooled. However, the degree of exchange may have limited the influence of ambient gas on chondrule oxygen isotope ratios (e.g. Schrader et al., 2013); this should be taken into consideration for model purposes. One way to assess the degree of exchange is to compare the oxygen isotope ratios of coexisting mineral phases in a chondrule. For instance, if exchange were inefficient, one might expect the oxygen isotope ratio of the chondrule melt to change over the duration of chondrule formation. Such a change would then be recorded in mineral phases that sequentially crystallized as the chondrule cooled (e.g. high to low temperature; olivine → low-Ca pyroxene → high-Ca pyroxene → plagioclase). However, $\Delta^{17}\text{O}$ values from almost all coexisting olivine, pyroxene, and plagioclase in type I CR3 chondrules agree to within analytical uncertainties (Fig. 10a). Similar results have been found in chondrules from Allende (CV3.6), Acfer 094 (ungr. C 3.00), and Yamato 81020 (CO3.05) chondrites (Rudraswami et al., 2011; Ushikubo et al., 2012; Tenner et al., 2013). In CR3 chondrules, olivines are slightly greater in $\delta^{18}\text{O}$ than coexisting pyroxenes and plagioclase (on average, by 0.7‰ ;

Table 3

Atomic abundances of H, O, and C in (1) CI dust; (2) H₂O depleted dusts used in the model shown in Fig. 11; and (3) examples of dust enriched assemblages.

	CI dust	dust with 0.8× ice	dust with 0.6× ice	dust with 0.4× ice	dust with 0.2× ice	dust with 0.1× ice	anhydrous dust
H	8.26×10^{6a}	6.61×10^6	4.95×10^6	3.30×10^6	1.65×10^6	8.26×10^5	0
O	7.63×10^6	6.80×10^6	5.97×10^6	5.14×10^6	4.31×10^6	3.90×10^6	3.50×10^6
C	7.56×10^5						
H/O	1.08	0.97	0.83	0.64	0.38	0.21	0
C/O	0.10	0.11	0.13	0.15	0.17	0.19	0.22
<i>O from: silicate in dust^b</i>	3.35×10^6						
<i>organics in dust^b</i>	1.51×10^5						
<i>H₂O ice in dust^b</i>	4.13×10^6	3.30×10^6	2.48×10^6	1.65×10^6	8.26×10^5	4.13×10^5	0
<i>100× dust enrichment^c</i>							
H	2.87×10^{10}	2.86×10^{10}	2.84×10^{10}	2.82×10^{10}	2.81×10^{10}	2.80×10^{10}	2.79×10^{10}
O	7.69×10^8	6.87×10^8	6.06×10^8	5.24×10^8	4.42×10^8	4.01×10^8	3.60×10^8
C	8.17×10^7						
H/O	37.34	41.55	46.89	53.89	63.49	69.76	77.45
C/O	0.11	0.12	0.13	0.16	0.18	0.20	0.23
<i>log fO₂-log IW^d</i>	-2.96	-3.06	-3.17	-3.31	-3.48	-3.58	-3.70
<i>chondrule Mg#^e</i>	97.92	98.21	98.50	98.78	99.05	99.19	99.32
<i>frac. O from: Solar gas^f</i>	0.018	0.020	0.023	0.026	0.031	0.034	0.038
<i>silicate in dust^f</i>	0.431	0.483	0.548	0.633	0.750	0.827	0.921
<i>organics in dust^f</i>	0.019	0.022	0.025	0.029	0.034	0.037	0.042
<i>H₂O ice in dust^f</i>	0.532	0.476	0.405	0.312	0.185	0.102	0
<i>500× dust enrichment</i>							
H	3.20×10^{10}	3.12×10^{10}	3.04×10^{10}	2.95×10^{10}	2.87×10^{10}	2.83×10^{10}	2.79×10^{10}
O	3.82×10^9	3.41×10^9	3.00×10^9	2.58×10^9	2.17×10^9	1.97×10^9	1.76×10^9
C	3.84×10^8						
H/O	8.38	9.15	10.13	11.43	13.22	14.40	15.85
C/O	0.10	0.11	0.13	0.15	0.18	0.20	0.22
<i>log fO₂-log IW^d</i>	-1.79	-1.88	-1.98	-2.10	-2.25	-2.35	-2.46
<i>chondrule Mg#^e</i>	88.05	89.47	90.94	92.46	94.01	94.79	95.58
<i>frac. O from: Solar gas^f</i>	0.004	0.004	0.005	0.005	0.006	0.007	0.008
<i>silicate in dust^f</i>	0.437	0.490	0.558	0.647	0.769	0.850	0.949
<i>organics in dust^f</i>	0.020	0.022	0.025	0.029	0.035	0.038	0.043
<i>H₂O ice in dust^f</i>	0.539	0.484	0.413	0.319	0.190	0.105	0
<i>1000× dust enrichment</i>							
H	3.61×10^{10}	3.45×10^{10}	3.28×10^{10}	3.12×10^{10}	2.95×10^{10}	2.87×10^{10}	2.79×10^{10}
O	7.64×10^9	6.81×10^9	5.99×10^9	5.16×10^9	4.34×10^9	3.92×10^9	3.51×10^9
C	7.62×10^8						
H/O	4.73	5.07	5.49	6.05	6.82	7.32	7.95
C/O	0.10	0.11	0.13	0.15	0.18	0.19	0.22
<i>log fO₂-log IW^d</i>	-1.35	-1.42	-1.50	-1.61	-1.74	-1.82	-1.92
<i>chondrule Mg#^e</i>	76.73	79.01	81.47	84.14	87.01	88.53	90.10
<i>frac. O from: Solar gas^f</i>	0.002	0.002	0.002	0.003	0.003	0.003	0.004
<i>silicate in dust^f</i>	0.438	0.491	0.559	0.648	0.772	0.853	0.953
<i>organics in dust^f</i>	0.020	0.022	0.025	0.029	0.035	0.038	0.043
<i>H₂O ice in dust^f</i>	0.540	0.485	0.413	0.320	0.190	0.105	0

*Abundances of H, O, and C in dusts are normalized to 10^6 atoms of Si.

^a The reported H abundance in CI dust is modified from the Anders and Grevesse (1989) value (Table 2); details regarding this modification are given in Section 4.4 of the main text.

^b Calculations of abundances of O in the silicate, organic material, and H₂O components of CI dust are detailed in Section 4.4. For H₂O enhanced and depleted dusts, the O and H abundances associated with H₂O are calculated relative to those in CI dust.

^c Dust enriched compositions are calculated by adding $(n - 1)$ times the atomic abundances in a given dust to those from Solar gas (i.e. the Allende Prieto and Lambert (2001, 2002) values in Table 2), where n is the dust enrichment factor.

^d calculated using Eq. (3);

^e calculated using Eq. (4).

^f The total amount of O in a dust enriched assemblage is calculated as: 1.367×10^7 (from Solar gas) + $[n - 1] \times 3.350 \times 10^6$ (from silicate in dust) + $[n - 1] \times 1.512 \times 10^5$ (from organics in dust) + $[n - 1] \times \text{ice enhancement/depletion factor} \times 4.129 \times 10^6$ (from H₂O ice in dust). The fractions of oxygen from each source can then be determined.

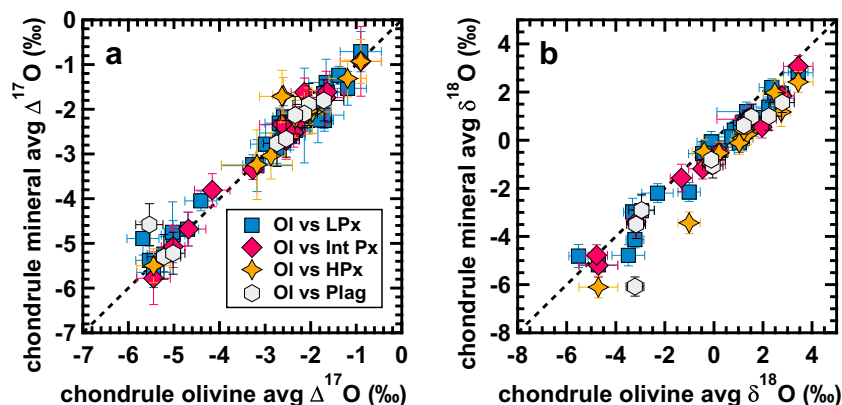


Fig. 10. (a) average $\Delta^{17}\text{O}$ and (b) average $\delta^{18}\text{O}$ comparisons between olivine and coexisting silicate mineral phases in CR3 chondrules. Each datum represents the averaged oxygen isotope ratio of olivine from a chondrule, and the average oxygen isotope ratio of the specified coexisting phase. Uncertainties are propagated 2SE. The dotted line in each panel indicates a one to one relationship. Ol: olivine; LPx: low-Ca pyroxene; Int Px: intermediate pyroxene; HPx: high-Ca pyroxene; Plag: plagioclase.

Appendix EA4; Fig. 10b). This tendency is also observed in Yamato 81020 chondrules (Tenner et al., 2013), and could represent inefficiency in oxygen isotope exchange between ambient gas and chondrule melt. However, an alternative explanation is that light O-isotopes from high-temperature chondrule melt preferentially evaporated before olivine crystallized. Following olivine crystallization and subsequent cooling, recondensation of light-isotope enriched ambient gas and/or kinetic isotope exchange involving ambient gas would have enriched the chondrule melt in light-isotopes, from which pyroxenes and plagioclase crystallized. If correct, the latter scenario would not detract from a conclusion of highly efficient oxygen isotope exchange between ambient gas and chondrule melt. Such a presumption is also supported by 1 atm. experiments from Yu et al. (1995), who demonstrate 80% exchange or more, in 30 min between H_2O vapor and chondrule melt during flash heating to 1450 °C, at cooling rates ≤ 480 °C/hr (for reference, typical chondrule cooling rates are estimated to be 100–1000 °C/hr; Hewins and Radomsky, 1990). Further, if chondrules formed by friction during shock heating (e.g. Desch et al., 2005), the imposed internal flow of chondrule melt (e.g. Uesugi et al., 2003) would increase molecular interactions between the melt and the surrounding gas, promoting high efficiency of O-isotope exchange. Therefore, when modeling chondrule oxygen isotope ratios we assume complete exchange between ambient gas and chondrule melt. A potential caveat to this assumption is that experiments by Boesenberg et al. (2005) indicate a lack of oxygen isotope exchange between CO gas and chondrule melt. However, catalytic phase equilibria, like Fischer–Tropsch reactions (Kress and Tielens, 2001; Barcena and Connolly, 2012), may have allowed for oxygen associated with carbon to influence chondrule oxygen isotope ratios. Although the exact degree of exchange is not clear, our assumption that CO in ambient gas exchanged completely with chondrule melt does not significantly affect our model, as the fraction of oxygen associated with carbon in ambient gas is small (e.g. Table 3).

4.5. Dust enrichment models

Using Eqs. (3)–(5), chondrule Mg# and $\Delta^{17}\text{O}$ model trends are generated as a function of dust enrichment and/or ice enhancement, and are compared to actual CR3 chondrule data. Here, we assess parameters of the environment from which CR chondrules formed.

Though essentially non-existent at high dust enrichment factors, oxygen from Solar gas may constitute percent levels of chondrule precursors at low dust enrichments (e.g. Table 3), and therefore could appreciably influence type I chondrule oxygen isotope ratios. We evaluate this in Fig. 11. At low CI dust enrichments ($<100\times$) the model predicts decreasing chondrule $\Delta^{17}\text{O}$ values with decreasing dust enrichment factors, due to an increasing proportion of ^{16}O -rich Solar gas in the precursor. However, the CI dust enrichment trend (the uppermost trend in Fig. 11) is too ^{16}O -poor when compared to the type I CR3 chondrule data, which suggests that changes in the dust to Solar gas ratio cannot fully explain the relationship between CR chondrule Mg#'s and their oxygen isotope ratios.

It is worth mentioning that at dust enrichments greater than $100\times$ the model essentially predicts constant $\Delta^{17}\text{O}$ values as a function of Mg#. This occurs because with increasing dust enrichment the fraction of oxygen from Solar gas becomes vanishingly small in the chondrule precursor (e.g. Table 3). As such, the oxygen isotope ratio of the precursor simply approaches the bulk value of the dust. Further, within the dust, the proportion of oxygen from organic matter is low (e.g. Table 3), meaning that at dust enrichments exceeding $100\times$ the oxygen isotope ratio of the precursor is predominantly controlled by (1) the O-isotope ratios of silicate and H_2O ice in the dust, and (2) the proportions of silicate and H_2O ice in the dust.

The limited role of Solar gas on CR chondrule Mg#'s and oxygen isotope ratios indicates other aspects of the environment must have accounted for their signatures. One possibility is that high Mg# CR chondrule precursors simply had less ^{16}O -poor H_2O ice in their dust, when compared to their lower Mg# counterparts. To explore this, we

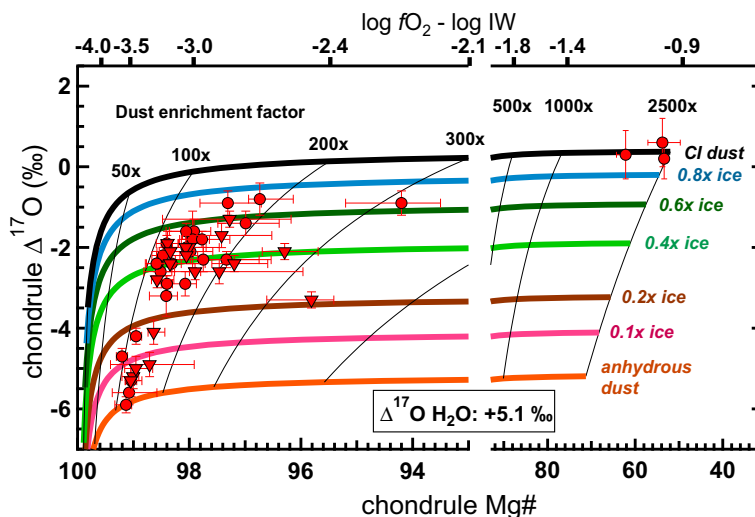


Fig. 11. Dust enrichment model and comparisons to CR3 chondrule data (red circles: MET 00426 chondrules; inverted red triangles: QUE 99177 chondrules). Using the composition of an assemblage at a specific dust enrichment factor (e.g. Table 3; thin semi-vertical lines) the imposed oxygen fugacity and chondrule Mg# are estimated (Eqs. (3) and (4), respectively). Fractions of oxygen from sources in the precursor are also calculated (e.g. Table 3), and when combined with specified $\Delta^{17}\text{O}$ values for each source, the bulk $\Delta^{17}\text{O}$ value of a chondrule is determined by mass balance (Eq. (5); thick horizontal lines). In the model, $\Delta^{17}\text{O}$ values of Solar gas, organic material in the dust, H_2O in the dust, and silicate in the dust are -28.4‰ , $+11.3\text{‰}$, $+5.1\text{‰}$, and -5.9‰ , respectively; details regarding these values are found in Section 4.4. Models employ dust enrichments exceeding $12.5\times$, the minimum condition necessary to stabilize a silicate liquid at a P^{tot} of 10^{-3} bar (Ebel and Grossman, 2000). Dust compositions (e.g. Table 3) used to generate respective dust enriched trends are labeled on the right side of the panel. Ice abundances in dusts are calculated relative to the atomic abundance in CI dust. (For interpretation of the references to colour in this figure legend, the reader is referred to the web version of this article.)

produce several dust compositions that are depleted in H_2O ice, relative to the atomic abundance in CI dust (Table 3). This allows for generating a family of ice-depleted dust enrichment trends that can be compared to CR3 chondrule data (Fig. 11). A notable aspect of the model is that at a fixed dust enrichment factor, increased ice enhancement of the dust yields increased chondrule $\Delta^{17}\text{O}$ values and decreased chondrule Mg#'s (semi-vertical thin black lines in Fig. 11). Interestingly, these trends have similar curvatures to the high Mg# CR3 chondrule data. More importantly, they suggest the majority of type I CR chondrules formed at dust enrichments between $100\times$ and $200\times$, and from dusts with 0 to 0.8 times the atomic abundance of H_2O in CI dust; in particular, dust in the highest Mg# chondrule precursors may have been essentially anhydrous (Fig. 11). Within the model constraints, the type II CR3 chondrule fragments are estimated to have formed at CI dust enrichments near $2500\times$. According to dynamic models of the protoplanetary disk (e.g. Cassen, 2001; Cuzzi et al., 2001) such highly dust enriched environments (i.e. $>200\times$) were likely scarce, which could potentially explain why modal abundances of type II chondrules in CR chondrites are low ($<1\%$ of the chondrule population; Weisberg et al., 1993).

4.5.1. What if H_2O in the precursor had a different O-isotope ratio?

Although we believe the $\Delta^{17}\text{O}$ of H_2O in our model (i.e.: $+5.1\text{‰}$) is appropriate, it is admittedly an estimated value. Here, we assess how the model differs if H_2O has a higher or lower $\Delta^{17}\text{O}$ value, based on estimates found in the litera-

ture. Atomic abundances of assemblages used in the following models are located in Appendix EA6.

Regarding H_2O with increased $\Delta^{17}\text{O}$ (relative to $+5.1\text{‰}$) the net effect on the model is the prediction of a more anhydrous chondrule-forming environment, resulting in higher dust enrichment factors needed to form chondrules. An extreme case is illustrated in Fig. 12a, using the value of “primordial water” ($\Delta^{17}\text{O}$: $+80\text{‰}$) from SIMS measurements of cosmic symplectites in Acfer 094 (Sakamoto et al., 2007). In this scenario the model predicts that type I and type II chondrules originated from dusts with 0 to 0.06 times the atomic abundance of H_2O , relative to CI dust, that type I CR3 chondrules formed at dust enrichments of $100\times$ to $400\times$, and that the type II CR3 chondrule fragments formed at dust enrichments of $3000\times$ to $4000\times$. This model is not favorable because many chondrules, including type I chondrules, are predicted to form at dust enrichments exceeding $200\times$; as stated previously, such regions in the protoplanetary disk were probably rare. In addition, the Mg# and $\Delta^{17}\text{O}$ relationship that exists among CR chondrite chondrules and silicates from the comet Wild 2 (e.g. Nakashima et al., 2012 and references therein) could suggest a wetter CR chondrite accretion region.

Regarding H_2O with lower $\Delta^{17}\text{O}$ (relative to $+5.1\text{‰}$) the model generally predicts a more hydrous chondrule-forming environment and lower overall dust enrichment factors. This may seem favorable, but an issue arises as H_2O $\Delta^{17}\text{O}$ values approach those of the CR3 type II chondrule fragments ($\Delta^{17}\text{O}$: $\sim+0.4\text{‰}$) because predicted ice enhancements become extremely high. An example is shown in Fig. 12b using the estimated value of water from whole rock and

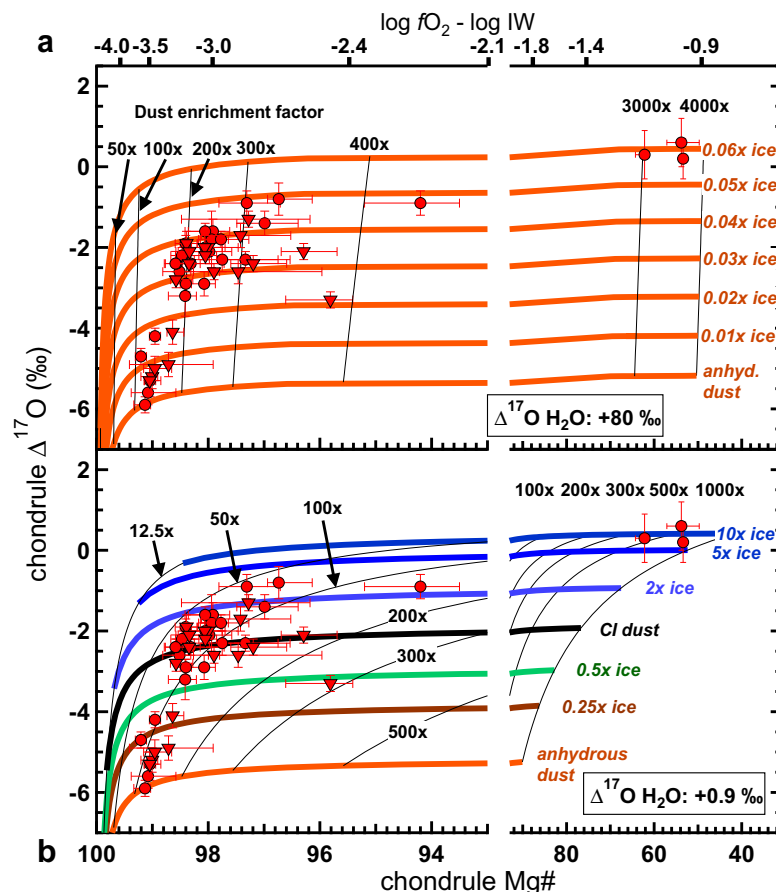


Fig. 12. Alternative dust enrichment models that employ different $\Delta^{17}\text{O}$ values for H_2O in the dust. The models are constructed using the same methods and parameters as described in the caption to Fig. 11, with the exception of the H_2O $\Delta^{17}\text{O}$ value. Color schemes correspond to those shown in Fig. 11. The top panel (a) uses the value of “primordial water” ($\Delta^{17}\text{O}:+80\text{‰}$) from measurements of cosmic symplectites in Acfer 094 by Sakamoto et al. (2007). The bottom panel (b) uses the value of “Light Water” ($\Delta^{17}\text{O}:+0.9\text{‰}$) estimated by Clayton and Mayeda (1999) from whole rock and matrix measurements in CR chondrites. (For interpretation of the references to colour in this figure legend, the reader is referred to the web version of this article.)

matrix measurements of CR chondrites by Clayton and Mayeda (1999) ($\Delta^{17}\text{O}:+0.9\text{‰}$). This model predicts similar dust enrichments (50–200 \times) and dust compositions (0 to 2 times the atomic abundance of ice, relative to CI dust) in the type I chondrule-forming environment when compared to the model in Fig. 11. However, it also predicts that the type II CR3 chondrule fragments would require dust with 10 times the atomic abundance of ice, relative to CI dust (Fig. 12b); this equates to a composition with an $\text{H}_2\text{O}:\text{SiO}_2$ ratio of 20 (i.e. 4.13×10^7 atoms of O associated with H_2O per 10^6 atoms of Si). This is probably unrealistically ice-enhanced, even when compared to comets. For example, spectral observations of the Deep Impact ejecta from comet 9P/Tempel 1 by Lisse et al. (2006) infer an atomic $\text{H}_2\text{O}:\text{SiO}_2$ ratio of 3.8, if assuming all H is H_2O and all Si is SiO_2 . Interestingly, Lisse et al. (2006) also suggest the comet ejecta composition is similar to CI dust, lending support to the use of CI dust to estimate H_2O $\Delta^{17}\text{O}$ (Section 4.4; Fig. 11). Overall, the issues with this particular model arise because of the assumption that all chondrules sampled H_2O with a single O-isotope ratio, based on the Mg# and $\Delta^{17}\text{O}$ relationship among CR3 chondrules (e.g. Fig. 7).

However, it cannot be ruled out that chondrule precursors sampled multiple H_2O reservoirs. If this was the case, then $\Delta^{17}\text{O} + 0.9\text{‰}$ H_2O could plausibly account for the formation of chondrules with $\Delta^{17}\text{O}$ values below $+0.4\text{‰}$, at more realistic dust compositions (i.e. CI dust; Fig. 12b).

4.6. Comparisons to chondrule data from other unequilibrated carbonaceous chondrites

Oxygen isotopes and Mg#'s of CR chondrules can be compared to data from unequilibrated Acfer 094, CO, and CV chondrites (Fig. 13), in order to infer similarities and/or differences within respective chondrule-forming environments. However, such a comparison is less than ideal for two reasons. First, datasets are often biased when compared to the representative distribution of chondrules from a given chondrite. This occurs because studies often focus on a group of chondrules with specific properties, or simply because samples may contain so many chondrules that acquiring a representative dataset is difficult. Second, CV chondrites experienced thermal metamorphism (e.g. Krot et al., 1998), which could modify primary chondrule

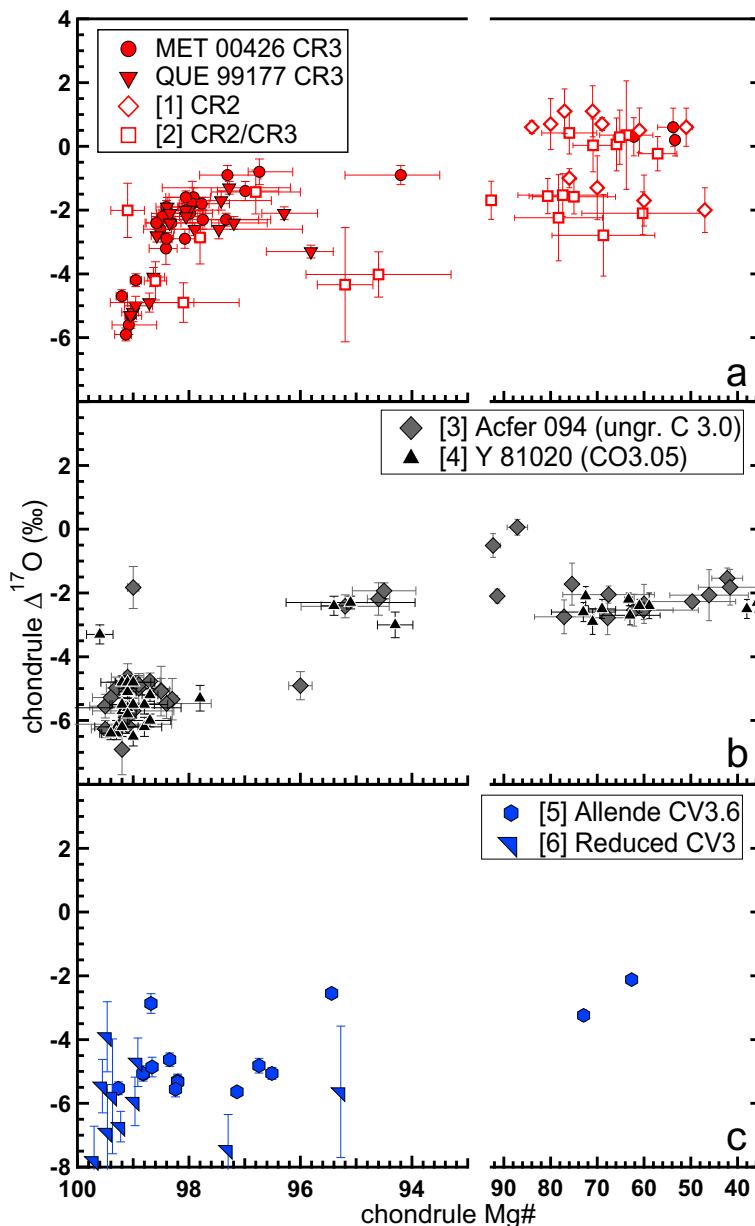


Fig. 13. Mg# and $\Delta^{17}\text{O}$ comparison of chondrules from carbonaceous chondrites. (a) CR chondrule data. [1] Connolly and Huss (2010) (open diamonds), [2] Schrader et al. (2013) (open squares) and this study (solid symbols). (b) Acfer 094 ([3]: Ushikubo et al., 2012) and Yamato 81020 CO3.05 ([4]: Tenner et al., 2013) chondrule data. (c) Allende CV3.6 chondrule data ([5]: Rudraswami et al., 2011), only from which Mg#'s can be calculated strictly from low-Ca pyroxene compositions. Reduced CV3 chondrule data from Efremovka and Vigarano ([6] Libourel and Chaussidon, 2011). In [1], [5], [6] uncertainties in respective Mg# are not reported; for [2], [3] and [4] the 1SD of Mg# data are shown.

signatures. While solid state oxygen diffusion is considerably slow in olivine and pyroxene at high temperatures (Cole and Chakraborty, 2001; Chakraborty, 2010), meaning their oxygen isotope ratios may not be disturbed during thermal metamorphism, Fe-Mg interdiffusion is sufficiently fast in olivine (e.g. Gerard and Jaoul, 1989), and their Mg#'s can be altered. For this reason we only consider Efremovka and Vigarano chondrule olivine data from Libourel and Chaussidon (2011), as these reduced CV chondrites experienced comparatively low amounts of

thermal metamorphism (petrographic type 3.1–3.4; Bonal et al., 2006). We also consider select Allende chondrule data from Rudraswami et al. (2011), where chondrule Mg#'s can be estimated from low-Ca pyroxene compositions. Although Allende has experienced a higher degree of thermal metamorphism ($\text{CV} > 3.6$; Bonal et al., 2006), the Fe–Mg interdiffusion rate of low-Ca pyroxene is at least two orders of magnitude lower than that of olivine (Ganguly and Tazzoli, 1994); therefore low-Ca pyroxene Mg#'s may retain primary chondrule Mg#'s.

Within the aforementioned limitations, the comparison of chondrule data from CR, Acfer 094, CO, and CV chondrites provides interesting results. Notably, many chondrules from each have Mg#’s greater than 98, while also having $\Delta^{17}\text{O}$ values of -4‰ to -6‰ (Fig. 13a–c). This indicates the presence of a highly reduced oxygen isotope reservoir that was commonly sampled by each carbonaceous chondrite.

In addition to ^{16}O -rich, high Mg# chondrules, CR, Acfer 094, CO, and CV chondrites have lower Mg# chondrules that are relatively ^{16}O -poor, with $\Delta^{17}\text{O}$ values mainly near -2‰ and 0‰ (Fig. 13). Within the limits of measurements, CR chondrites appear to have sampled both O-isotope reservoirs (Fig. 13a), while Acfer 094, CO3, and CV3 chondrites primarily have lower Mg# chondrules with $\Delta^{17}\text{O}$ values near -2‰ (Fig. 13b and c). Collectively, the predominance of lower Mg# chondrules with values of $\sim 0\text{‰}$ or -2‰ could suggest two distinct environments of high dust enrichment that differed with respect to the abundance of ice in the dust (e.g. Fig. 11). Alternatively, or in conjunction, these two environments could have sampled two isotopically distinct H_2O reservoirs. Another possibility is a difference in the efficiency of oxygen isotope exchange between ambient gas and chondrule melt, as suggested by Schrader et al. (2013). Finally, it is worth mentioning that several type II chondrules from carbonaceous chondrites have Mg#’s less than the composition of CI chondrites (54.3) (Fig. 13a and b), meaning their precursors were likely Fe-rich when compared to CI dust.

4.7. Implications regarding the dynamics of the carbonaceous chondrite accretion region

In carbonaceous chondrites, the majority of chondrules (75–99%; e.g. Weisberg et al., 1993; Krot et al., 2002b; Kunihiro et al., 2005; Scott and Krot, 2007) are FeO-poor, with Mg#’s greater than 90. Many have Mg#’s exceeding 98, implying formation at dust enrichments less than $200\times$ (e.g. Fig. 11). Combined, these characteristics match dynamic disk evolution models, which predict that more than 70% of the protoplanetary disk had dust enrichment factors under $200\times$ (Cuzzi et al., 2001; Cassen, 2001). Therefore, many chondrules from carbonaceous chondrites could have formed by a pervasive process (e.g. Boss, 1996; Connolly and Love, 1998; Desch and Cuzzi, 2000; Ciesla and Hood, 2002; Ciesla et al., 2004; Cuzzi and Alexander, 2006), from a common $\Delta^{17}\text{O}$: -4‰ to -6‰ oxygen isotope reservoir (e.g. Fig. 13). The type I CR chondrule-forming environment may have been unique when compared to those from other carbonaceous chondrites, because at least some portion (specifically, that which formed $> \Delta^{17}\text{O}$: -4 to -6‰ type I chondrules) was relatively enhanced in H_2O ice (Figs. 11 and 13). This could indicate that CR chondrites accreted at greater heliocentric distances than other carbonaceous chondrites. Within the constraints of our model, abundances of H_2O within type I and type II chondrule-forming environments (e.g. Fig. 11) do not overstep the amount of potential H_2O transported to the inner disk by icy materials. For example, Ciesla and Cuzzi (2006) calculate a maximum H_2O enhancement of approximately

ten times the Solar composition, corresponding to $\sim 4.8 \times 10^7$ atoms of O per 10^6 atoms of Si, if using methods from Krot et al. (2000) (15% of O in Solar gas is bound to “rocky” components and all C is bound to O), and the composition from Allende Prieto and Lambert (2001, 2002). In contrast, the abundance of O associated with H_2O in a CI dust enriched assemblage, $\sim 4.13 \times 10^6$ atoms per 10^6 atoms of Si (Table 3), is significantly lower, and for ice-depleted dusts the abundance is even less.

The lower modal proportion of type II chondrules in carbonaceous chondrites (1–25%) suggests a different, and more limited chondrule-forming environment that was likely enhanced in dust and H_2O ice (e.g. Fig. 11). The suggested dust enrichment factors and/or ice enhancements required to form type II chondrules, from this study and others (e.g. Fedkin and Grossman, 2006; Grossman et al., 2012; Fedkin et al., 2012), are difficult to explain within the context of dynamic models. Perhaps localized regions of high dust enrichment (only 5–30% of the protoplanetary disk exceeded $200\times$; Cuzzi et al., 2001) accompanied by significant ice enhancement could have imposed a temporary, oxidized environment that could form type II chondrules through an early Solar system process (e.g. Ciesla et al., 2003; Alexander et al., 2008; Fedkin et al., 2012; Sanders and Scott, 2012).

Finally, while the constraints we use to model chondrule formation are appropriate for CR chondrites, and could be applicable to other carbonaceous chondrites, we caution against their use to model the formation of chondrules in other chondrites (ordinary, enstatite, R, etc.). Specifically, it is not unreasonable that such environments could have differed with respect to the fractions of components in their chondrule precursors, and/or that the components could have sampled different oxygen isotope reservoirs. Therefore, such parameters would need to be carefully assessed and implemented.

5. CONCLUSIONS

Detailed Mg#’s by EMP analysis and in-situ oxygen three-isotope ratios by SIMS were determined in chondrules from the highly unequilibrated CR3.00 chondrites MET 00426 and QUE 99177. The main conclusions are:

- (1) The majority of chondrules/fragments (45 of 48) are FeO-poor (type I), consistent with findings by Weisberg et al. (1993) in CR2 chondrites. Chondrule Mg#’s (defined as the Mg#’s of their constituent olivine and/or low-Ca pyroxene) range from 94.2 to 99.2. O-isotope measurements plot along the primitive chondrule mineral (PCM) line defined by chondrules in Acfer 094 (Ushikubo et al., 2012). Within most chondrules/fragments, O-isotope ratios of coexisting olivine, pyroxene, and plagioclase are homogeneous, indicating (a) they crystallized from the final chondrule melt; and (b) that O-isotope exchange between ambient gas and the chondrule melt was highly efficient. Among chondrules/fragments there is a well-defined increase in chondrule $\Delta^{17}\text{O}$, from -5.9‰ to $\sim -1\text{‰}$ (typical uncertainty: 0.3‰), as chondrule

Mg#’s decrease from 99.2 to ~96. To the best of our knowledge, this is the first time such a trend has been observed among chondrules within a single chondrite group.

- (2) Three type II chondrule fragments, with Mg#’s of 53.4, 53.8, and 62.2, have O-isotopes that lie along the PCM line, and are ^{16}O -poor relative to type I chondrules, with $\Delta^{17}\text{O}$ values of 0.2–0.6‰. Although similar in $\Delta^{17}\text{O}$, they are ~1‰ greater in $\delta^{18}\text{O}$ when compared to type II chondrule data from LL3 chondrites measured by Kita et al. (2010).
- (3) The continuous increase in type I CR3 chondrule $\Delta^{17}\text{O}$ with decreasing chondrule Mg# supports the hypothesis from Connolly and Huss (2010) that addition of ^{16}O -poor H_2O ice to type I chondrule precursors, when combined with increasing dust enrichment, aided in forming type II CR chondrules.
- (4) Using aspects of existing equilibrium condensation models (Ebel and Grossman, 2000; Fedkin and Grossman, 2006; Grossman et al., 2008) and a simple O-isotope mass balance, the conditions of dust enrichment and/or H_2O enhancement necessary to explain the CR3 chondrule Mg# versus $\Delta^{17}\text{O}$ trend were evaluated. We predict type I CR chondrules formed at dust enrichments between 100× and 200×, and that dust in their precursors had 0 to 0.8 times the atomic abundance of H_2O , relative to CI dust. In addition, we estimate that the type II chondrule fragments formed at CI dust enrichments near 2500×. According to dynamic models (e.g. Cassen, 2001; Cuzzi et al., 2001) environments with dust enrichments exceeding 200× were likely scarce in the protoplanetary disk, which may explain the low abundance of type II chondrules in CR chondrites.
- (5) Chondrules in carbonaceous chondrites are predominantly FeO-poor (Mg# > 90; 75–99% modally), of which many have $\Delta^{17}\text{O}$ values of –4 to –6‰. This indicates the presence of a reduced and commonly sampled O-isotope reservoir. Combined with the prevalence of low dust enrichment conditions in the protoplanetary disk (i.e. greater than 70% existed at less than 200×; Cassen, 2001; Cuzzi et al., 2001) and suggested abundances of ice well-within the potential amounts delivered by icy migrators (e.g. Ciesla and Cuzzi, 2006), the majority of type I chondrules from carbonaceous chondrites could have formed by a common, pervasive process.
- (6) Type II chondrules from carbonaceous chondrites mainly have $\Delta^{17}\text{O}$ values of ~0‰ and ~–2‰. This indicates two distinct environments of high dust enrichment that could have differed in terms of the abundance of ^{16}O -poor H_2O ice in their precursors, and/or sampling of two distinct H_2O ice oxygen isotope reservoirs, and/or different efficiencies of isotope exchange between ambient gas and chondrule melt. CR chondrites sampled both chondrule-forming environments (e.g. Connolly and Huss, 2010; Schrader et al., 2013; this study). The low modal abundance of type II chondrules in carbonaceous chondrites (1–25%), when combined with high dust

enrichment factors and relatively high abundances of H_2O necessary for their formation, could indicate the presence of a different, and more limited chondrule-forming environment, with a different formation process than type I chondrules.

ACKNOWLEDGEMENTS

We thank the ANSMET Program and Meteorite Working Group for allocating CR3 chondrite thin sections for this study. We thank John Fournelle for assistance with EMP analysis, and Jim Kern for technical assistance during SIMS operations. Constructive reviews were provided by Harold Connolly Jr., Yunbin Guan, Kazuhide Nagashima, and associate editor Dimitri Papanastassiou. This work is supported by the NASA Cosmochemistry program (NNX11AG62G, N.T.K.; NNX12AI06G, M.K.W.). WiscSIMS is partly supported by NSF (EAR03-19230, EAR07-44079, EAR10-53466).

APPENDIX A. SUPPLEMENTARY DATA

Supplementary data associated with this article can be found, in the online version, at <http://dx.doi.org/10.1016/j.gca.2014.09.025>.

REFERENCES

- Abreu N. M. and Brearley A. J. (2010) Early solar system processes recorded in the matrices of two highly pristine CR3 carbonaceous chondrites, MET 00426 and QUE 99177. *Geochim. Cosmochim. Acta* **74**, 1146–1171.
- Alexander C. M. O. D., Grossman J. N., Ebel D. S. and Ciesla F. J. (2008) The formation conditions of chondrules and chondrites. *Science* **320**, 1617–1619.
- Allende Prieto C. and Lambert D. L. (2001) The forbidden abundance of oxygen in the Sun. *Astrophys. J.* **556**, L63–L66.
- Allende Prieto C. and Lambert D. L. (2002) A reappraisal of the solar photospheric C/O ratio. *Astrophys. J.* **573**, L137–L140.
- Anders E. and Grevesse N. (1989) Abundances of the elements: meteoritic and solar. *Geochim. Cosmochim. Acta* **53**, 197–214.
- Baertschi P. (1976) Absolute ^{18}O content of standard mean ocean water. *Earth Planet. Sci. Lett.* **31**, 341–344.
- Barcena H. and Connolly Jr., H. C. (2012) Constraining the nature of type-I chondrules: I. chemical models. *43rd Lunar and Planet. Sci. Conf.* CD-ROM. #2506 (abstr.).
- Beatty D. W. and Albee A. L. (1980) Silica solid solution and zoning in natural plagioclase. *Am. Miner.* **65**, 63–74.
- Binet L., Gourier D., Derenne S. and Robert F. (2002) Heterogeneous distribution of paramagnetic radicals in insoluble organic matter from the Orgueil and Murchison meteorites. *Geochim. Cosmochim. Acta* **66**, 4177–4186.
- Boesenberg J. S., Young E. D., Ziegler K. and Hewins R. H. (2005) Evaporation and the absence of oxygen isotopic exchange between silicate melt and carbon monoxide gas at nebular pressures. *Meteorit. Planet. Sci.* **40**, A22 (abstr.).
- Bonal L., Quirico E., Bourot-Denise M. and Montagnac G. (2006) Determination of the petrologic type of CV3 chondrites by Raman spectroscopy of included organic matter. *Geochim. Cosmochim. Acta* **70**, 1849–1863.
- Boss A. P. (1996) A concise guide to chondrule formation models. In *Chondrules and the Protoplanetary Disk* (eds. R. H. Hewins,

- R. H. Jones and E. R. D. Scott). Cambridge Univ. Press, Cambridge, pp. 257–293.
- Cassen P. (2001) Nebular thermal evolution and the properties of primitive planetary materials. *Meteorit. Planet. Sci.* **36**, 671–700.
- Chakraborty S. (2010) Diffusion coefficients in olivine, wadsleyite, and ringwoodite. In *Reviews in Mineralogy and Geochemistry*, 72 (eds. Y. Zhang and D. J. Cherniak). Mineralogical Society of America, Washington, DC, pp. 603–639.
- Chakraborty S., Yanchulova P. and Thiemens M. H. (2013) Mass-independent oxygen isotopic partitioning during gas-phase SiO₂ formation. *Science* **342**, 463–466.
- Ciesla F. J. and Hood L. L. (2002) The nebular shock wave model for chondrule formation: shock processing in a particle-gas suspension. *Icarus* **158**, 281–293.
- Ciesla F. J. and Cuzzi J. N. (2006) The evolution of the water distribution in a viscous protoplanetary disk. *Icarus* **181**, 178–204.
- Ciesla F. J., Lauretta D. S., Cohen B. A. and Hood L. L. (2003) A nebular origin for chondritic fine-grained phyllosilicates. *Science* **299**, 549–552.
- Ciesla F. J., Hood L. L. and Weidenschilling S. J. (2004) Evaluating planetesimal bow shocks as sites for chondrule formation. *Meteorit. Planet. Sci.* **39**, 1809–1821.
- Clayton R. N. (1993) Oxygen isotopes in meteorites. *Ann. Rev. Earth Planet. Sci.* **21**, 115–149.
- Clayton R. N. and Mayeda T. K. (1999) Oxygen isotope studies of carbonaceous chondrites. *Geochim. Cosmochim. Acta* **63**, 2089–2104.
- Clayton R. N., Onuma N., Grossman L. and Mayeda T. K. (1977) Distribution of the pre-solar component in Allende and other carbonaceous chondrites. *Earth Planet. Sci. Lett.* **34**, 209–224.
- Clayton R.N., Onuma N., Ikeda Y., Mayeda T.K., Hutcheon I.D., Olsen E.J., and Molini-Velsko C. (1983) Oxygen isotopic compositions of chondrules in Allende and ordinary chondrites. In *Chondrules and their Origins* (ed. E. A. King), pp. 37–43.
- Clayton R. N., Mayeda T. K., Goswami J. N. and Olsen E. J. (1991) Oxygen isotope studies of ordinary chondrites. *Geochim. Cosmochim. Acta* **55**, 2317–2337.
- Cole D. R. and Chakraborty S. (2001) Rates and mechanisms of isotope exchange. In *Reviews in Mineralogy and Geochemistry*, 43 (eds. J. W. Valley and D. R. Cole). Mineralogical Society of America, Washington D.C., pp. 83–223.
- Connolly, Jr., H. C. and Huss G. R. (2010) Compositional evolution of the protoplanetary disk: oxygen isotopes of type-II chondrules from CR2 chondrites. *Geochim. Cosmochim. Acta* **74**, 2473–2483.
- Connolly, Jr., H. C., Hewins R. H., Ash R. D., Zanda B., Lofgren G. E. and Bourrot-Denise M. (1994) Carbon and the formation of reduced chondrules. *Nature* **371**, 136–139.
- Connolly, Jr., H. C. and Love S. G. (1998) The formation of chondrules: petrologic tests of the shock wave model. *Science* **280**, 62–67.
- Cuzzi J. N. and Zahnle K. J. (2004) Material enhancement in protoplanetary nebulae by particle drift through evaporation fronts. *Astrophys. J.* **614**, 490–496.
- Cuzzi J. N. and Alexander C. M. O. D. (2006) Chondrule formation in particle-rich nebular regions at least hundreds of kilometers across. *Nature* **441**, 483–485.
- Cuzzi J. N., Hogan R. C., Paque J. M. and Dobrovolskis A. R. (2001) Size-selective concentration of chondrules and other small particles in protoplanetary nebula turbulence. *Astrophys. J.* **546**, 496–508.
- Desch S. J. and Cuzzi J. N. (2000) The generation of lightning in the solar nebula. *Icarus* **143**, 87–105.
- Desch S. J. and Connolly, Jr., H. C. (2002) A model of the thermal processing of particles in solar nebula shocks: application to the cooling rates of chondrules. *Meteorit. Planet. Sci.* **37**, 183–207.
- Desch S. J., Ciesla F. J., Hood L. L. and Nakamoto T. (2005) Heating of chondritic materials in solar nebula shocks. In *ASP Conference Series 341, Chondrites and the Protoplanetary Disk* (eds. A. N. Krot, E. R. D. Sott and B. Reipurth). Astronomical Society of the Pacific, San Francisco, CA, pp. 849–872.
- Ebel D. S. and Grossman L. (2000) Condensation in dust-enriched systems. *Geochim. Cosmochim. Acta* **64**, 339–366.
- Ebel D. S., Ghiorso M. S., Sack R. O. and Grossman L. (1999) Gibbs energy minimization in gas + liquid + solid systems. *J. Comput. Chem.* **21**, 247–256.
- Ebel D. S., Weisberg M. K., Hertz J. and Campbell A. J. (2008) Shape, metal abundance, chemistry, and origin of chondrules in the Renazzo (CR) chondrite. *Meteorit. Planet. Sci.* **43**, 1725–1740.
- Fedkin A. V. and Grossman L. (2006) The fayalite content of chondritic olivine: obstacle to understanding the condensation of rocky material. In *Meteorites and the Early Solar System II* (eds. D. S. Lauretta and H. Y. McSween). Univ. of Arizona Press, Tuscon, pp. 279–294.
- Fedkin A. V., Grossman L., Ciesla F. J. and Simon S. B. (2012) Mineralogical and isotopic constraints on chondrule formation from shock wave thermal histories. *Geochim. Cosmochim. Acta* **87**, 81–116.
- Ganguly J. and Tazzoli V. (1994) Fe²⁺–Mg interdiffusion in orthopyroxene: retrieval from the data on intracrystalline exchange reaction. *Am. Miner.* **79**, 930–937.
- Gerard O. and Jaoul O. (1989) Oxygen diffusion in San-Carlos olivine. *J. Geophys. Res.* **94**, 4119–4128.
- Ghiorso M. S. and Sack R. O. (1995) Chemical mass transfer in magmatic processes IV. A revised and internally consistent thermodynamic model for the interpolation and extrapolation of liquid-solid equilibria in magmatic systems at elevated temperatures and pressures. *Contrib. Mineral. Petrol.* **119**, 197–212.
- Gounelle M., Krot A. N., Nagashima K. and Kearsley A. (2009) Extreme ¹⁶O enrichment in calcium-aluminum-rich inclusions from the Isheyevo (CH/CB) chondrite. *Astrophys. J.* **698**, L18–L22.
- Grossman J. N. and Brearley A. J. (2005) The onset of metamorphism in ordinary and carbonaceous chondrites. *Meteorit. Planet. Sci.* **40**, 87–122.
- Grossman L., Beckett J. R., Fedkin A. V., Simon S. B. and Ciesla F. J. (2008) Redox conditions in the solar nebula: observational, experimental, and theoretical constraints. In *Reviews in Mineralogy and Geochemistry*, 68 (ed. G. J. MacPherson). Mineralogical Society of America, Washington, DC, pp. 93–140.
- Grossman L., Fedkin A. V. and Simon S. B. (2012) Formation of the first oxidized iron in the solar system. *Meteorit. Planet. Sci.* **47**, 2160–2169.
- Hashizume K., Takahata N., Naraoka H. and Sano Y. (2011) Extreme oxygen isotope anomaly with a solar origin detected in meteoritic organics. *Nature Geosci.* **4**, 165–168.
- Heck P. R., Ushikubo T., Schmitz B., Kita N. T., Spicuzza M. J. and Valley J. W. (2010) A single asteroidal source for extraterrestrial Ordovician chromite grains from Sweden and China: high-precision oxygen three-isotope SIMS analysis. *Geochim. Cosmochim. Acta* **74**, 497–509.
- Hewins R. H. and Radomsky P. M. (1990) Temperature conditions for chondrule formation. *Meteoritics* **25**, 309–318.
- Jones R. H. (1990) Petrology and mineralogy of type II, FeO-rich chondrules in Semarkona (LL3.0): origin by closed-system

- fractional crystallization, with evidence for supercooling. *Geochim. Cosmochim. Acta* **54**, 1785–1802.
- Jones R. H. (1994) Petrology of FeO-poor, porphyritic pyroxene chondrules in the Semarkona chondrite. *Geochim. Cosmochim. Acta* **58**, 5325–5340.
- Jones R. H. (1996) FeO-rich, porphyritic pyroxene chondrules in unequilibrated ordinary chondrites. *Geochim. Cosmochim. Acta* **60**, 3115–3138.
- Jones R. H. and Scott E. R. D. (1989) Petrology and thermal history of type IA chondrules in the Semarkona (LL3.0) chondrite. *Proc. 19th Lunar Planet. Sci. Conf.*, 523–536.
- Jones R. H. and Schilk A. J. (2009) Chemistry, petrology and bulk oxygen isotope compositions of chondrules from the Mokoia CV3 carbonaceous chondrite. *Geochim. Cosmochim. Acta* **73**, 5854–5883.
- Jones R. H., Saxton J. M., Lyon I. C. and Turner G. (2000) Oxygen isotopes in chondrule olivine and isolated olivine grains from the CO3 chondrule Allan Hills A77307. *Meteorit. Planet. Sci.* **35**, 849–857.
- Jones R. H., Leshin L. A., Guan Y., Sharp Z. D., Durakiewicz T. and Schilk A. J. (2004) Oxygen isotope heterogeneity in chondrules from the Mokoia CV3 carbonaceous chondrite. *Geochim. Cosmochim. Acta* **68**, 3423–3438.
- Jones R. H., Grossman G. N. and Rubin A. E. (2005) Chemical, mineralogical, and isotopic properties of chondrules: clues to their origins. In *Chondrites and the Protoplanetary Disk* (eds. A.N. Krot, E.R.D. Scott and B. Reipurth). Astronomical Society of the Pacific Conference Series 341, pp. 251–286.
- Kallemeyn G. W., Rubin A. E. and Wasson J. T. (1994) The compositional classification of chondrites: VI. The CR carbonaceous chondrite group. *Geochim. Cosmochim. Acta* **58**, 2873–2888.
- Kita N. T., Ushikubo T., Fu B. and Valley J. W. (2009) High precision SIMS oxygen isotope analysis and the effect of sample topography. *Chem. Geol.* **264**, 43–57.
- Kita N. T., Nagahara H., Tachibana S., Tomomura S., Spicuzza M. J., Fournelle J. H. and Valley J. W. (2010) High precision SIMS oxygen three isotope study of chondrules in LL3 chondrites: role of ambient gas during chondrule formation. *Geochim. Cosmochim. Acta* **74**, 6610–6635.
- Kobayashi S., Imai H. and Yurimoto H. (2003) New extreme ^{16}O -rich reservoir in the early solar system. *Geochim. J.* **37**, 663–669.
- Kress M. E. and Tielens A. G. G. M. (2001) The role of Fischer–Tropsch catalysis in solar nebula chemistry. *Meteorit. Planet. Sci.* **36**, 75–91.
- Kring D. A. (1988) The petrology of meteoritic chondrules: evidence for fluctuating conditions in the solar nebula. PhD thesis, Harvard Univ.
- Krot A. N., Petaev M. I., Scott E. D., Choi B.-G., Zolensky M. E. and Keil K. (1998) Progressive alteration in CV3 chondrites: more evidence for asteroidal alteration. *Meteorit. Planet. Sci.* **33**, 1065–1085.
- Krot A. N., Fegley, Jr., B., Lodders K. and Palme H. (2000) Meteoritic and astrophysical constraints on the oxidation state of the solar nebula. In *Protostars and Planets IV* (eds. V. Mannings, et al.). Univ. of Arizona, Tuscon, pp. 1019–1054.
- Krot A. N., Meibom A., Weisberg M. K. and Keil K. (2002a) The CR chondrite clan: implications for early solar system processes. *Meteorit. Planet. Sci.* **37**, 1451–1490.
- Krot A. N., Hutcheon I. D. and Keil K. (2002b) Plagioclase-rich chondrules in the reduced CV chondrites: evidence for complex formation history and genetic links between calcium-aluminum-rich inclusions and ferromagnesian chondrules. *Meteorit. Planet. Sci.* **37**, 155–182.
- Krot A. N., Yurimoto H., McKeegan K. D., Leshin L., Chaussidon M., Libourel G., Yoshitake M., Huss G. R., Guan Y. and Zanda B. (2006a) Oxygen isotopic compositions of chondrules: implications for evolution of oxygen isotopic reservoirs in the inner solar nebula. *Chem. Erde* **66**, 249–276.
- Krot A. N., Libourel G. and Chaussidon M. (2006b) Oxygen isotope compositions of chondrules in CR chondrites. *Geochim. Cosmochim. Acta* **70**, 767–779.
- Krot A. N., Nagashima K., Yoshitake M. and Yurimoto H. (2010) Oxygen isotopic compositions of chondrules from the metal-rich chondrites Isheyev (CH/CB_b), MAC 02675 (CB_b) and QUE 94627 (CB_b). *Geochim. Cosmochim. Acta* **74**, 2190–2211.
- Kunihiro T., Rubin A. E., McKeegan K. D. and Wasson J. T. (2004) Oxygen-isotopic compositions of relict and host grains in chondrules in the Yamato 81020 CO3.0 chondrite. *Geochim. Cosmochim. Acta* **68**, 3599–3606.
- Kunihiro T., Rubin A. E. and Wasson J. T. (2005) Oxygen-isotopic compositions of low-FeO relicts in high FeO-host chondrules in Acfer 094, a type 3.0 carbonaceous chondrite closely related to CM. *Geochim. Cosmochim. Acta* **69**, 3831–3840.
- Kurahashi E., Kita N. T., Nagahara H. and Morishita Y. (2008) ^{26}Al – ^{26}Mg systematics of chondrules in a primitive CO chondrite. *Geochim. Cosmochim. Acta* **72**, 3865–3882.
- Libourel G. and Chaussidon M. (2011) Oxygen isotopic constraints on the origin of Mg-rich olivines from chondritic meteorites. *Earth Planet. Sci. Lett.* **301**, 9–21.
- Lisse C. M., VanCleve J., Adams A. C., A’Hearn M. F., Fernández Y. R., Farnham T. L., Armus L., Grillmair C. J., Ingalls J., Belton M. J. S., Groussin O., McFadden L. A., Meech K. J., Schultz P. H., Clark B. C., Feaga L. M. and Sunshine J. M. (2006) Spitzer spectral observations of the Deep Impact ejecta. *Science* **313**, 635–640.
- Lyons J. R. and Young E. D. (2005) CO self-shielding as the origin of oxygen isotope anomalies in the early solar nebula. *Nature* **435**, 317–320.
- Lyons J. R., Bergin E. A., Ciesla F. J., Davis A. M., Desch S. J., Hashizume K. and Lee J.-E. (2009) Timescales for the evolution of oxygen isotope compositions in the solar nebula. *Geochim. Cosmochim. Acta* **73**, 4998–5017.
- McKeegan K. D., Kallio A. P. A., Heber V. S., Jarzembinski G., Mao P. H., Coath C. D., Kunihiro T., Wiens R. C., Nordholt J. E., Moses R. W., Reisenfeld D. B., Jurewicz A. J. G. and Burnett D. S. (2011) The oxygen isotopic composition of the Sun inferred from captured solar wind. *Science* **332**, 1528–1532.
- McSween H. Y. (1977) Chemical and petrographic constraints on the origin of chondrules and inclusions in carbonaceous chondrites. *Geochim. Cosmochim. Acta* **41**, 1843–1860.
- Nakashima D., Kimura M., Yamada K., Noguchi T., Ushikubo T. and Kita N. T. (2010) Study of chondrules in CH chondrites – I: oxygen isotope ratios of chondrules. *Meteorit. Planet. Sci. Suppl.* **45**, A148 (abstr.).
- Nakashima D., Ushikubo T., Joswiak D. J., Brownlee D. E., Matrajt G., Weisberg M. K., Zolensky M. E. and Kita N. T. (2012) Oxygen isotopes in crystalline silicates of comet Wild 2: a comparison of oxygen isotope systematics between Wild 2 particles and chondritic materials. *Earth Planet. Sci. Lett.* **357–358**, 355–365.
- Remusat L., Robert F. and Derenne S. (2007) The insoluble organic matter in carbonaceous chondrites: chemical structure, isotopic composition and origin. *C. R. Geosci.* **339**, 895–906.
- Rubin A. E. and Wasson J. T. (1995) Variations of chondrite properties with heliocentric distance. *Meteoritics* **30**, A569 (abstr.).
- Rudraswami N. G., Ushikubo T., Nakashima D. and Kita N. T. (2011) Oxygen isotope systematics of chondrules in the Allende

- CV3 chondrite: high precision ion microprobe studies. *Geochim. Cosmochim. Acta* **75**, 7596–7611.
- Sakamoto N., Seto Y., Itoh S., Kuramoto K., Fujino K., Nagashima K., Krot A. N. and Yurimoto H. (2007) Remnants of the early solar system water enriched in heavy oxygen isotopes. *Science* **317**, 231–233.
- Sanders I. S. and Scott E. R. D. (2012) The origin of chondrules and chondrites: debris from low-velocity impacts between molten planetesimals? *Meteorit. Planet. Sci.* **47**, 2170–2192.
- Schrader D. L., Connolly, Jr., H. C., Lauretta D. S., Nagashima K., Huss G. R., Davidson J. and Domanik K. J. (2013) The formation and alteration of the Renazzo-like carbonaceous chondrites II: linking O-isotope composition and oxidation state of chondrule olivine. *Geochim. Cosmochim. Acta* **101**, 302–327.
- Scott E. R. D. and Jones R. H. (1990) Disentangling nebular and asteroidal features of CO3 carbonaceous chondrite meteorites. *Geochim. Cosmochim. Acta* **54**, 2485–2502.
- Scott E. R. D., Love S. G. and Krot A. N. (1996) Formation of chondrules and chondrites in the protoplanetary nebula. In *Chondrules and the Protoplanetary Disk* (eds. R. H. Hewins, R. H. Jones and E. R. D. Scott). Cambridge Univ. Press, Cambridge, pp. 87–96.
- Scott E. R. D. and Krot A. N. (2007) Chondrites and their components. In *Meteorites, Comets and Planets* (ed. A.M. Davis), Treatise on Geochemistry vol. 1. pp. 143–200.
- Tachibana S., Nagahara H., Mostefaoui S. and Kita N. T. (2003) Correlation between relative ages inferred from ^{26}Al and bulk compositions of ferromagnesian chondrules in least equilibrated ordinary chondrites. *Meteorit. Planet. Sci.* **38**, 939–962.
- Tenner T. J., Ushikubo T., Kurahashi E., Kita N. T. and Nagahara H. (2013) Oxygen isotope systematics of chondrule phenocrysts from the CO3.0 chondrite Yamato 81020: evidence for two distinct oxygen isotope reservoirs. *Geochim. Cosmochim. Acta* **102**, 226–245.
- Thiemens M. H. and Heidenreich J. E. (1983) The mass-independent fractionation of oxygen—a novel isotope effect and its possible cosmochemical implications. *Science* **219**, 1073–1075.
- Tsuchiyama A., Nagahara H. and Kushiro I. (1980) Experimental reproduction of textures of chondrules. *Earth Planet. Sci. Lett.* **48**, 155–165.
- Uesugi M., Sekiya M. and Nakamoto T. (2003) Deformation and internal flow of a chondrule-precursor sphere in a shocked nebula gas. *Earth Planet. Space* **55**, 493–507.
- Ushikubo T., Kimura M., Kita N. T. and Valley J. W. (2012) Primordial oxygen isotope reservoirs of the solar nebula recorded in chondrules in Acfer 094 carbonaceous chondrite. *Geochim. Cosmochim. Acta* **90**, 242–264.
- Wasson J. T., Rubin A. E. and Yurimoto H. (2004) Evidence in CO3.0 chondrules for a drift in the O isotopic composition of the solar nebula. *Meteorit. Planet. Sci.* **39**, 1591–1598.
- Weisberg M. K., Prinz M., Clayton R. N. and Mayeda T. K. (1993) The CR (Renazzo-type) carbonaceous chondrite group and its implications. *Geochim. Cosmochim. Acta* **57**, 1567–1586.
- Weisberg M. K., Ebel D. S., Connolly, Jr., H. C., Kita N. T. and Ushikubo T. (2011) Petrology and oxygen isotope compositions of chondrules in E3 chondrites. *Geochim. Cosmochim. Acta* **75**, 6556–6569.
- Wood J. A. (1967) Olivine and pyroxene compositions in Type II carbonaceous chondrites. *Geochim. Cosmochim. Acta* **31**, 2095–2108.
- Young E. D. and Russell S. S. (1998) Oxygen reservoirs in the early solar nebula inferred from an Allende CAI. *Science* **282**, 452–455.
- Young E. D., Kuramoto K., Marcus R. A., Yurimoto H. and Jacobsen S. B. (2008) Mass independent oxygen isotope variation in the solar nebula. In *Reviews in Mineralogy and Geochemistry*, 68 (ed. G. J. MacPherson). Mineralogical Society of America, Washington, D.C., pp. 187–218.
- Yu Y., Hewins R. H., Clayton R. N. and Mayeda T. K. (1995) Experimental study of high temperature oxygen isotope exchange during chondrule formation. *Geochim. Cosmochim. Acta* **59**, 2095–2104.
- Yurimoto H. and Kuramoto K. (2004) Molecular cloud origin for the oxygen isotope heterogeneity in the solar system. *Science* **305**, 1763–1766.
- Yurimoto H., Krot A. N., Choi B.-G., Aléon J., Kunihiro T. and Brearley A. J. (2008) Oxygen isotopes of chondritic components. In *Reviews in Mineralogy and Geochemistry*, 68 (ed. G. J. MacPherson). Mineralogical Society of America, Washington, D.C., pp. 141–186.
- Zanda B., Bourot-Denise M., Perron C. and Hewins R. H. (1994) Origin and metamorphic redistribution of silicon, chromium, and phosphorus in the metal of chondrites. *Science* **265**, 1846–1849.
- Zanda B., Bourot-Denise M., Hewins R. H., Cohen B. A., Delaney J. S., Humayun M. and Campbell A. J. (2002) Accretion textures, iron evaporation and re-condensation in Renazzo chondrules. *33rd Lunar and Planet. Sci. Conf.* CD-ROM. #1852 (abstr.).

Associate editor: Dimitri A. Papanastassiou